iScience

CellPress
OPEN ACCESS

Article

Mitochondrial complex I inhibitors suppress tumor growth through concomitant acidification of the intra- and extracellular environment

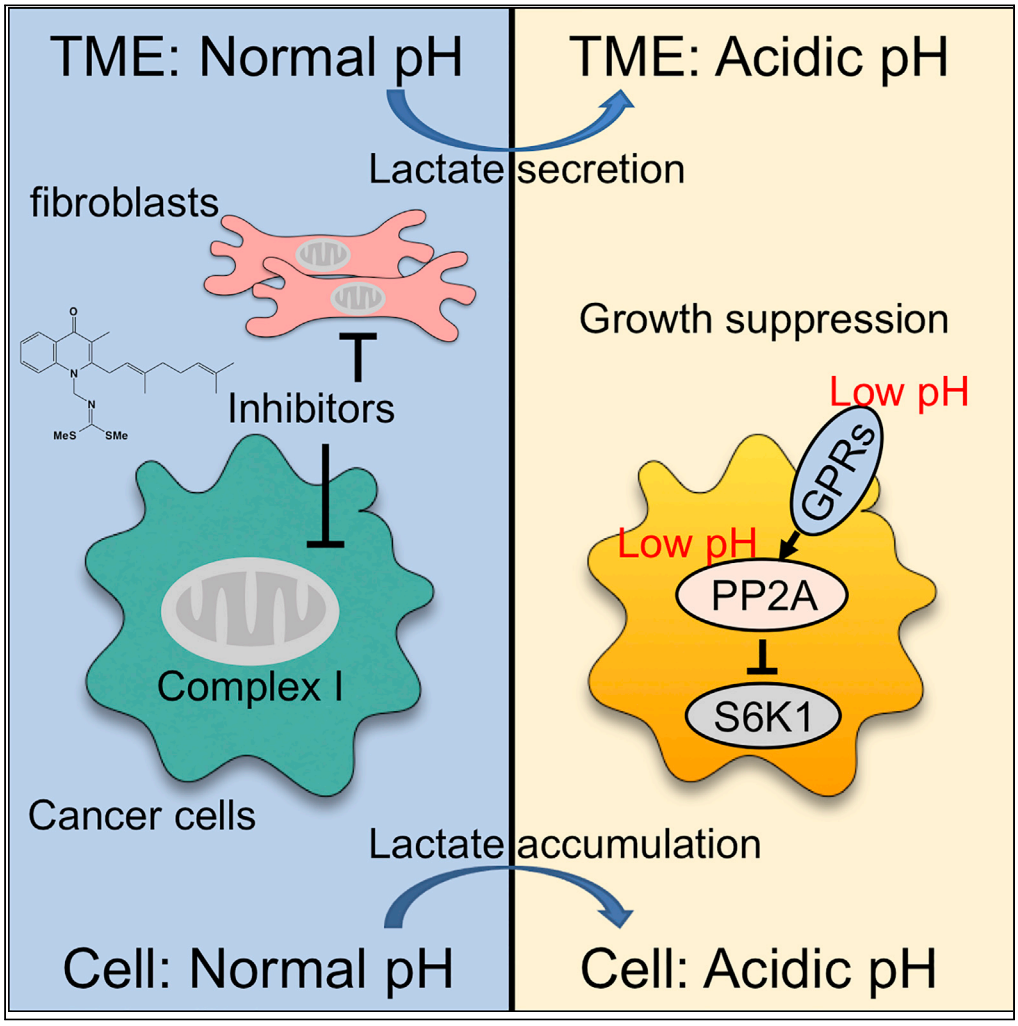

Junjiro Yoshida, Tomokazu Ohishi, Hikaru Abe, ..., Takao Shimizu, Masakatsu Shibasaki, Manabu Kawada

kawadam@bikaken.or.jp

Highlights

Stromal cells enhance anti-cancer activity of complex I inhibitors

Anti-cancer activity of complex I inhibitors is independent on energy depletion

Complex I inhibitors suppress S6K1 through the intra- and extracellular acidification

Acidic tumor microenvironment is more susceptible to complex I inhibitors

Yoshida et al., iScience 24, 103497
December 17, 2021
https://doi.org/10.1016/j.isci.2021.103497

iScience

CellPress
OPEN ACCESS

Article

Mitochondrial complex I inhibitors suppress tumor growth through concomitant acidification of the intra- and extracellular environment

Junjiro Yoshida,[1] Tomokazu Ohishi,[2] Hikaru Abe,[3] Shun-ichi Ohba,[2] Hiroyuki Inoue,[2] Ihomi Usami,[2] Masahide Amemiya,[1] Raphael Oriez,[3] Chiharu Sakashita,[3] Shingo Dan,[4] Minoru Sugawara,[5] Tokuichi Kawaguchi,[5] Junko Ueno,[6] Yuko Asano,[6] Ami Ikeda,[6] Manabu Takamatsu,[7,8] Gulanbar Amori,[7,8] Yasumitsu Kondoh,[9] Kaori Honda,[9] Hiroyuki Osada,[9] Tetsuo Noda,[10] Takumi Watanabe,[3] Takao Shimizu,[11,12,13] Masakatsu Shibasaki,[3] and Manabu Kawada[1,2,14,*]

SUMMARY

The disruption of the tumor microenvironment (TME) is a promising anti-cancer strategy, but its effective targeting for solid tumors remains unknown. Here, we investigated the anti-cancer activity of the mitochondrial complex I inhibitor intervenolin (ITV), which modulates the TME independent of energy depletion. By modulating lactate metabolism, ITV induced the concomitant acidification of the intra- and extracellular environment, which synergistically suppressed S6K1 activity in cancer cells through protein phosphatase-2A-mediated dephosphorylation via G-protein-coupled receptor(s). Other complex I inhibitors including metformin and rotenone were also found to exert the same effect through an energy depletion-independent manner as ITV. In mouse and patient-derived xenograft models, ITV was found to suppress tumor growth and its mode of action was further confirmed. The TME is usually acidic owing to glycolytic cancer cell metabolism, and this condition is more susceptible to complex I inhibitors. Thus, we have demonstrated a potential treatment strategy for solid tumors.

INTRODUCTION

Tumor tissues contain cancer cells and several stromal cells, such as macrophages (Hao et al., 2018; Mantovani et al., 2017), vascular endothelial cells (Hida et al., 2004; Huang et al., 2019), immune cells (Lambrechts et al., 2018; Lavin et al., 2017), and fibroblasts (Kalluri, 2016; Mizutani et al., 2019). Among stromal cells in tumor tissues, cancer-associated fibroblasts (CAFs) produce cytokines, growth factors, and various proteins that constitute the extracellular matrix to support the proliferation of cancer cells (Erez et al., 2010; Kawada et al., 2015; Tian et al., 2019; Zhang et al., 2018). Such a tumor-supportive environment is established by not only these proteins but also metabolites from CAFs that are induced by tumor-stromal cell interactions to support the metabolic energy production of cancer cells in response to lower nutrient conditions in the tumor microenvironment (TME). The oncogenic TME makes cancer cells reliant on specific energy metabolism or proliferative signaling pathways (Eckert et al., 2019; Sousa et al., 2016). Thus, disruption of the TME can lead to the suppression of cancer cells adapted to the TME. Therefore, the TME is a target for cancer therapy, and a more detailed understanding of TME modulation could provide effective strategies for tumor suppression.

Thus, we focused on the TME, especially cancer-stromal cell interactions, to identify anti-cancer drug targets and detected many compounds, such as bacterial and fungal metabolites, from natural sources with potential anti-cancer activity (Kawada et al., 2009a, 2009b, 2010a, 2010b). Recently, we discovered a novel natural compound called intervenolin (ITV) from the culture medium of *Nocardia* sp. ML96-86F2 and evaluated its anti-cancer activity in a co-culture system of cancer and stromal cells (Kawada et al., 2013). We found that ITV suppresses gastric cancer cell growth upon co-culture with gastric fibroblasts and exhibits higher suppressive activity than in monoculture conditions (Yoshida et al., 2018). In addition, the conditioned medium (CM) of fibroblasts treated with ITV exhibited anti-cancer activity. Thus, we proposed that ITV suppresses cancer cell growth via direct and indirect mechanisms, the latter involving fibroblasts.

[1]Laboratory of Oncology, Institute of Microbial Chemistry (BIKAKEN), Shinagawa-ku, Tokyo 141-0021, Japan

[2]Numazu Branch and Section of Animal Resources, Institute of Microbial Chemistry (BIKAKEN), Numazu-shi, Shizuoka 410-0301, Japan

[3]Laboratory of Synthetic Organic Chemistry, Institute of Microbial Chemistry (BIKAKEN), Shinagawa-ku, Tokyo 141-0021, Japan

[4]Division of Molecular Pharmacology, Cancer Chemotherapy Center, Japanese Foundation for Cancer Research, Koto-ku, Tokyo 135-8550, Japan

[5]Cancer Precision Medicine Center, Japanese Foundation for Cancer Research, Koto-ku, Tokyo 135-8550, Japan

[6]Department of Cancer Genomics, Cancer Institute, Japanese Foundation for Cancer Research, Koto-ku, Tokyo 135-8550, Japan

[7]Division of Pathology, Cancer Institute, Japanese Foundation for Cancer Research, Koto-ku, Tokyo 135-8550, Japan

[8]Department of Pathology, Cancer Institute Hospital, Japanese Foundation for Cancer Research, Koto-ku, Tokyo 135-8550, Japan

[9]Chemical Biology Research Group & Drug Discovery Chemical Bank Unit, RIKEN Center for Sustainable Resource Science, Wako, Saitama 351-0198, Japan

[10]Director's Room, Cancer Institute, Japanese Foundation for Cancer

Continued

Interestingly, in the present study, we found that ITV is a potent mitochondrial complex I inhibitor. Compounds with complex I inhibitor mechanisms have been evaluated as anti-cancer drugs (Ashton et al., 2018). For instance, the anti-cancer activity of metformin, a well-known biguanide clinically used as a first-line therapy for type 2 diabetes, has been extensively studied (Pernicova and Korbonits, 2014). Metformin activates adenosine 5′-adenosine monophosphate-activated protein kinase (AMPK) via ATP reduction through the inhibition of mitochondrial complex I activity, thus leading to the inhibition of the mammalian target of rapamycin complex 1 (mTORC1) signaling, an important cascade in cancer growth (Hardie, 2014; Zhou et al., 2019). In accordance with these findings, ASP4132, another complex I inhibitor, exhibits anti-cancer activity by activating AMPK (Kuramoto et al., 2020). However, recent studies have identified novel targets of metformin whose mode of action is independent of AMPK (Kalender et al., 2010). Therefore, the anti-cancer activity of complex I inhibitors remains to be fully elucidated.

Recently, treatment with IACS-010759, a clinical-grade small molecule inhibitor of OXPHOS via mitochondrial complex I inhibition, was found to deplete the energy and suppress the growth of glioblastoma and leukemia cells, whose growth depends on oxidative phosphorylation (OXPHOS) for energy production (Molina et al., 2018). Currently, a phase I trial of IACS-010759 for patients with advanced solid tumors, relapsed/refractory acute myeloid leukemia, and lymphomas is underway. Thus far, IACS-010759 has a favorable safety profile (NCT02882321 and NCT03291938). Accordingly, OXPHOS has emerged as a target for treating these OXPHOS-dependent cancers (Ashton et al., 2018).

Therefore, to elucidate the direct and indirect mechanisms underlying the anti-cancer activity of ITV and mitochondrial complex I inhibitors, we analyzed the changes in the extracellular environment following the inhibition of complex I. We employed metabolic analyses of the extra- and intracellular environments and analyzed the cancer-suppressive signaling pathways related to the metabolic shift in cancer cell lines and studied mouse and patient-derived xenograft (PDX) models to determine the anti-cancer mechanism of mitochondrial complex I inhibitors.

RESULTS

Anti-tumor activity of ITV is potentiated in co-culture conditions

First, we investigated the effect of ITV on gastric cancer cells co-cultured with gastric stromal cells. We confirmed that ITV (Figure 1A) significantly suppresses the growth of gastric cancer cell lines MKN-B and MKN-74 upon co-culture with gastric stromal cells (Hs738) at lower concentrations than in monoculture conditions (Figures 1B and S1A). As ITV also exhibited stronger growth inhibitory activity against cancer cells in non-contact co-culture experiments than in monoculture (Yoshida et al., 2018), we speculated that ITV exerts growth suppression on cancer cells by modulating extracellular conditions. Indeed, MKN-1, MKN-B, and MKN-74 cell growth was suppressed by the CM of stromal cells pre-treated with ITV (ITV CM) (Figures 1C, 1D, and S1B), thus indicating indirect ITV activity.

The enhancement of ITV anti-cancer activity upon co-culture was further validated in several cancer cell lines from other organs, including the colon, lung, prostate, and pancreas, paired with stromal cells originating from the same organs. We found that ITV exhibited growth inhibitory activity against not only gastric cancer cell lines but also other cancer cell lines from different organs (Figure S1C) and that this inhibitory activity is significantly potentiated in co-culture conditions. These results suggest that ITV exhibits anti-cancer activity by regulating extracellular conditions.

ITV suppresses tumor growth in a mouse xenograft model

We further evaluated the anti-tumor activity of ITV against MKN-74 cells inoculated with or without Hs738 cells to determine whether stromal cells can enhance anti-tumor activity *in vivo*. Upon ITV treatment, mice bearing MKN-74 and Hs738 cells had significantly reduced tumor growth, tumor weight, and Ki-67 positivity without body weight loss at day 21 (Figures 1E, 1F, S2B, and S2C). Tumor growth was also suppressed by ITV treatment at the same extent in mice bearing MKN-74 alone (Figures 1F, S2A, and S2D).

Histochemical and immunohistochemical analysis results showed that fibroblast-like stromal cells are abundant in the tumor tissues regardless of co-inoculation with Hs738 cells (Figures 1E, and S2A). Fibroblast-like cells in tumors from mice bearing MKN-74 cells alone are predicted to be derived from host mice. Consequently, MKN-74 cell growth was significantly inhibited by ITV treatment upon co-culture with isolated mouse fibroblasts compared with that in monoculture conditions (Figure 1G). These results

Research, Koto-ku, Tokyo 135-8550, Japan

[11]Department of Lipid Signaling, Research Institute, National Center for Global Health and Medicine, Shinjuku-ku, Tokyo 162-8655, Japan

[12]Department of Lipidomics, Graduate School of Medicine, The University of Tokyo, Tokyo 113-0033, Japan

[13]Laboratory of Virology, Institute of Microbial Chemistry (BIKAKEN), Shinagawa-ku, Tokyo 141-0021, Japan

[14]Lead contact

*Correspondence:: kawadam@bikaken.or.jp

https://doi.org/10.1016/j.isci.2021.103497

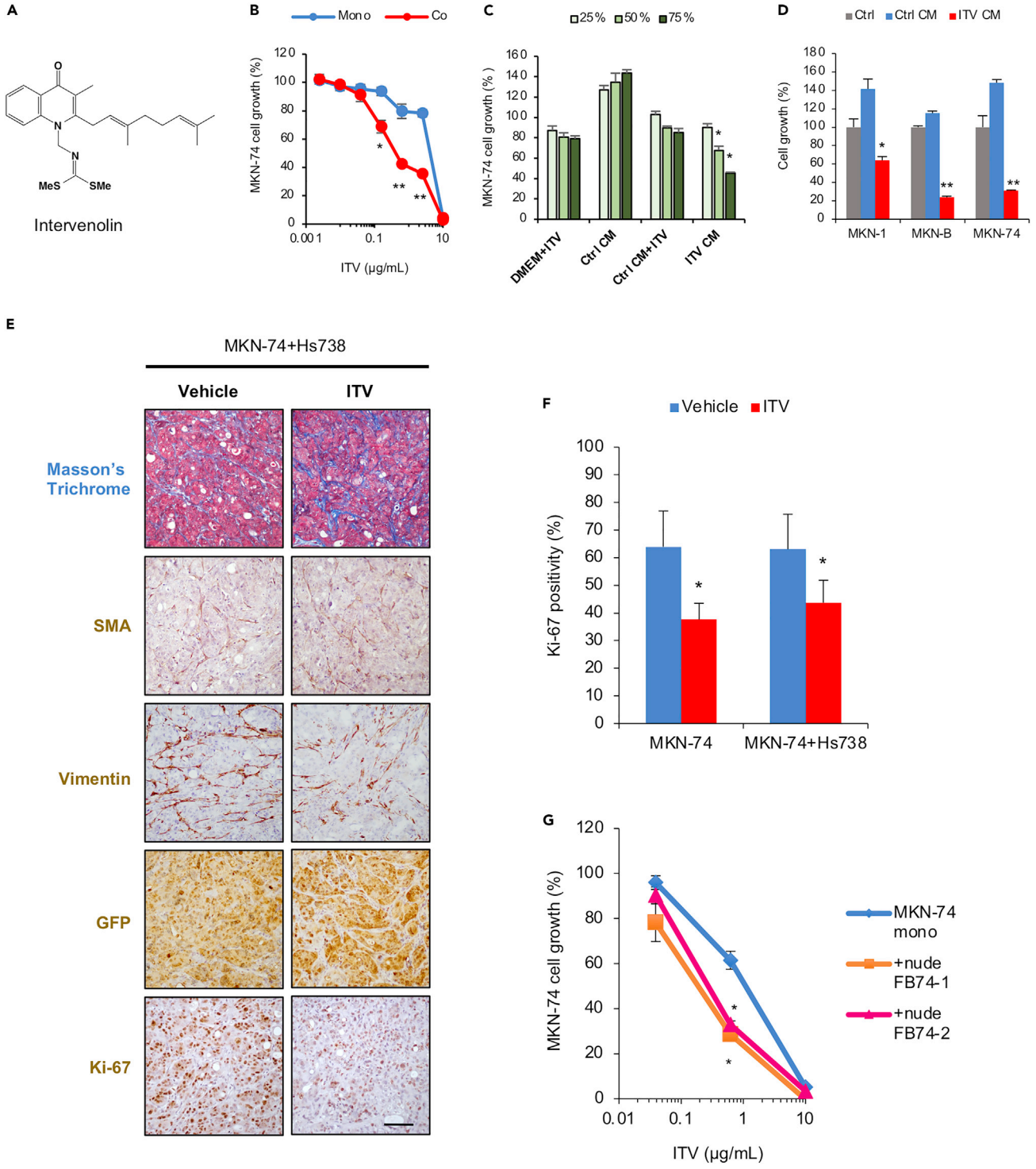

Figure 1. Intervenolin (ITV) exhibits anti-cancer activity that is potentiated in co-culture conditions

(A) Structure of ITV.

(B) Growth of MKN-74 cells cultured alone (Mono) or with Hs738 (Co) for 3 days at the indicated ITV concentrations were measured using GFP fluorescence intensity and expressed as percentage relative to that of cells without ITV treatment (n = 3; *$p < 0.005$, **$p < 0.001$ versus mono).

(C) Growth of MKN-74 cells upon treatment with ITV CM, Ctrl CM, and their respective controls (DMEM + ITV and Ctrl CM + ITV) for 3 days (*$p < 0.001$ versus Ctrl CM+ ITV). For each condition, 1 μg/mL ITV was used.

(D) Growth of cancer cell lines MKN-1, -B, and –74 (n = 3).

Figure 1. *Continued*

(E) Formalin-fixed, paraffin-embedded tumor sections from mice inoculated with MKN-74 and Hs738 cells treated with the vehicle or 12.5 mg/kg ITV were stained with Masson's trichrome stain and analyzed using immunohistochemistry with antibodies against the indicated proteins. Scale bar, 100 μm (n = 5).

(F) Percentages of Ki-67-positive cells in the high-power field of tumor sections (n = 5; *$p < 0.01$).

(G) MKN-74 cells were cultured alone (Mono) or with fibroblast cells isolated from mice tumor tissues (+nude FB74-1,2) (Co) for 3 days in the presence of ITV at the indicated concentrations (n = 3; *$p < 0.0005$ versus mono).

Data are presented as the mean ± SD and were analyzed using two-sided Student's t test.

indicate that ITV suppresses cancer cell growth by modulating the TME *in vivo* regardless of the origin of stromal cells.

Mode of action of ITV

Using a panel of 39 human cancer cell lines (termed JFCR39), we predicted the mechanism of action of several compounds by comparing the fingerprint of GI_{50} (half growth inhibition) against JFCR39 with 250 reference compounds (Dan et al., 2002; Paull et al., 1989; Yamori, 2003). Some biguanide compounds showed high correlation with ITV in the JFCR39 system (buformin: r = 0.737; phenformin: r = 0.696; metformin: r = 0.586) (Figure S2E). Buformin and phenformin are derivatives of metformin, which is the first alternative drug for type 2 diabetes. Biguanides and metformin are also anti-cancer reagents, which function primarily by inhibiting mitochondrial complex I.

Next, we examined whether complex I inhibition is essential for the anti-cancer activity of ITV and found that all complex I inhibitors, including buformin, metformin, arctigenin, and rotenone (Bridges et al., 2014; Ravanel et al., 1984; Thomas et al., 2013), exhibit significantly stronger growth inhibitory activities against gastric cancer cells upon co-culture with Hs738 than in monoculture, similar to ITV (Figure S2F). This suggests that ITV is a possible complex I inhibitor and that mitochondrial complex I inhibition is required for its enhanced anti-cancer activity in the presence of stromal cells.

ITV inhibits mitochondrial complex I activity

We evaluated the potential of ITV as a complex I inhibitor by measuring oxidative consumption rate (OCR) and found that ITV significantly suppresses OCR and reactivity against FCCP, an uncoupler, in a dose-dependent manner (Figures 2A and S3A). Although glucose supplementation upregulated OCR of gastric cancer cells in glucose- and pyruvate-depleted control, ITV or rotenone (positive control as a complex I inhibitor) maintained low OCR levels even in the presence of sufficient glucose, but this inhibition was reversed by succinate supplementation (Figures S3B and S3C). Succinate is a substrate of complex II and can partially bypass the function of complex I (Ehinger et al., 2016).

We further evaluated ITV inhibitory activity against the enzymatic activity of complex I using isolated mitochondria and observed that ITV more strongly inhibits complex I activity than do biguanides, such as buformin and metformin (Figures 2B, S3D, and S3E). Results of enzymatic analysis of complexes II, II/III, IV, and V showed that ITV does not inhibit other components of the electron transport chain (ETC) and OXPHOS (Figure S3F) up to 1 μg/mL.

Next, ITV binding to a target molecule was examined using pull-down assays; as AS-1936 is an ITV derivative and its inhibition of cancer cell growth is not potentiated in co-culture conditions, it was used as a control with a significantly lower activity (Figure S4A). NDUFB8, a subunit of complex I, coprecipitated with ITV, which was inhibited by excess ITV (Figure S4B), indicating that ITV binds and inhibits mitochondrial complex I. Because ITV (1 μg/mL), metformin (1,000 μg/mL), and rotenone (0.01 μg/mL) suppressed the OCR of gastric cancer cells to the same extent, the OCR values were well correlated with their inhibitory activity in co-culture conditions (Figures S4C and S4D).

Complex I inhibitory activity against MKN-B, MKN-74, and Hs738 cells showed no significant difference; thus, we speculated that target cells of ITV in the co-culture environment are both stromal and gastric cancer cells (Figures 2B, S3D, and S3E).

ITV increases extracellular lactate levels via metabolic shift

We determined the factor(s) present in the ITV-treated cell culture medium and found that ITV upregulates the extracellular acidification rate (ECAR) of cancer cells. According to the OCR and ECAR energy map of

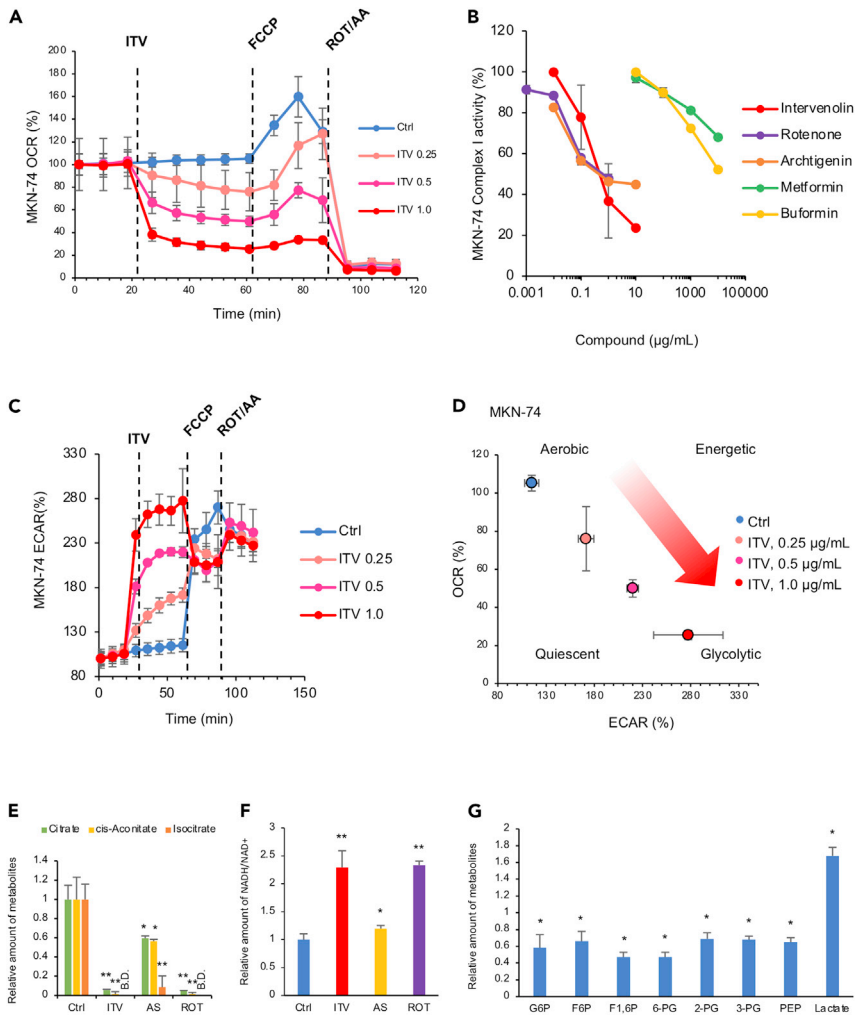

Figure 2. Intervenolin (ITV) inhibits mitochondrial complex I activity and induces metabolic shift in cancer cells

(A) Results of seahorse flux analyzer assays showing the OCR of MKN-74 cells. Assay buffer (Ctrl) or the indicated concentrations of ITV were introduced at 24 min; FCCP, 64 min; and rotenone (ROT) and antimycin A (AA), 88 min.

(B) Activity of the mitochondrial complex I as measured using an NADH assay. Reduction rate of NADH that normalized by non-treated value was shown as complex I activity. The activity of mitochondria without compounds was defined as 100%.

(C) Seahorse flux analyzer assay results showing the extracellular acidification rate (ECAR) in MKN-74 cells as in (A).

(D) Energy map of MKN-74 cells based on OCR and ECAR values. The status of the metabolic pathways is classified as aerobic, glycolytic, energetic, or quiescent.

(E–G). Intracellular metabolite concentrations were determined using mass spectrometric analysis (E and F). Relative amounts of the indicated metabolites in MKN-74 cells treated by 1 μg/mL ITV, 1 μg/mL AS-1936 (AS), or 0.01 μg/mL rotenone (ROT) for 3 h are shown. B.D., below detection limit ($n = 3$; *$p < 0.05$ versus Ctrl, **$p < 0.005$ versus Ctrl).

(G) Relative amounts of the indicated metabolites in MKN-74 cells treated by ITV for 3 h are shown ($n = 3$; *$p < 0.05$ versus non-treated cells). Data are presented as the mean ± SD ($n = 3$) and normalized according to the baseline and analyzed using two-sided Student's t -test.

ITV-treated gastric cancer cells, energy production shifted to glycolysis to compensate for OXPHOS inhibition (Figures 2C, 2D, S4E, and S4F). Therefore, we speculated that metabolite(s) are involved in ITV CM activity.

We thus performed metabolomic analysis to clarify the metabolomic changes caused by ITV and other complex I inhibitors. We focused on glycolysis and the tricarboxylic acid (TCA) cycle because metabolites involved in these pathways were significantly altered (Figure S5). ITV or rotenone reduced the levels of the components of the TCA cycle, such as citrate, *cis*-aconitate, and isocitrate, to a lesser extent than did

AS-1936 (Figure 2E). As the NADH/NAD+ ratio in MKN-74 cells treated with ITV or rotenone was significantly upregulated, we attributed the downregulation of the TCA cycle to the suppressed consumption of NADH due to complex I inhibition (Figure 2F). Levels of the intermediate metabolites of glycolysis, such as G6P, F6P, F1, 6P, 6-PG, 2-PG, 3-PG, and PEP, were reduced by ITV, but those of its end product, lactate, were elevated (Figure 2G). The decrease in intermediate metabolite levels compensated for the ITV- or rotenone-induced OXPHOS inhibition, and the increase in lactate levels was due to the suppression of the TCA cycle.

In accordance with these findings, the extracellular lactate levels in co-culture conditions were significantly greater (>10 mM) than in monocultures (3–5 mM at 0.6 μg/mL ITV) (Figure S6A). Moreover, ITV, metformin, and rotenone significantly increased lactate levels and decreased glucose levels in the CM of Hs738 cells compared with MKN-B and MKN-74 cells (Figures S6B–S6D). Thus, these results suggest that lactate is a candidate factor involved in the mechanism of ITV anti-cancer activity. Furthermore, the reduction in both intra- and extracellular nutrient levels caused by metabolic changes cannot be a critical factor for the anti-cancer activity of ITV in co-culture conditions as nutrient supplementation, such as with glutamine, pyruvate, and glucose, did not attenuate ITV CM activity (Figure S6E).

S6K1 is synergistically downregulated by extracellular acidification and complex I inhibition

We next evaluated whether the addition of lactate with ITV suppresses cancer cell growth. However, we observed that sodium lactate does not inhibit gastric cancer cell growth even in the presence of ITV, metformin, or rotenone (Figures S6F–S6I). We then investigated the environmental factors influencing the anti-cancer property of ITV. Interestingly, ITV CM had a lower pH (pH 6.9) than the control medium (pH 7.4) or control CM (pH 7.4) from Hs738. Therefore, we evaluated whether acidic conditions potentiate the anti-cancer activity of ITV and found that gastric cancer cell growth is inhibited at low pH even with ITV treatment (pH/ITV) at the same extent as with ITV CM (Figure 3A). However, pH neutralization suppressed the growth inhibitory activity of pH/ITV and ITV CM against cancer cells (Figure 3A). Hence, extracellular acidification caused by elevated lactate levels enhances the anti-cancer activity of ITV.

Next, we performed an anti-phospho-kinase antibody array to determine the intracellular signals involved in ITV-induced cell growth inhibition. Some kinases such as Akt (S473), ERK1/2 (T202/Y204), AMPKα1 (T172), and S6K1 (T389) were determined as suppressed targets of ITV CM (Figures S7A, S7B, and Table S1). Glucose levels in the ITV CM was significantly lower than in the control CM (Figures S6C and S6D). Immunoblot analysis showed that excess glucose recovered the phosphorylation status of Akt, ERK1/2, and AMPKα1 but not S6K1 (Figure S7B) and did not suppress the growth inhibitory activity of ITV CM (Figure S7C). Furthermore, ITV, but not AS-1936, suppressed S6K1 phosphorylation in gastric cancer cells cultured under acidic conditions (10 mM lactate supplementation and low pH medium) but not in 10 mM sodium lactate (Figures 3B and 3D). Similar results were observed using metformin and rotenone (Figure 3B). S6K1 was significantly suppressed in the ITV CM (Figure 3C). Therefore, potentiated ITV (or complex I inhibitors) action under acidic conditions due to elevated lactate levels suppresses S6K1, inhibiting tumor cell growth.

Suppression of S6K1 phosphorylation is protein phosphatase-2A dependent

S6K1 activity is necessary for protein synthesis, and the AMPK/mTORC1 pathway is a well-known S6K1-suppressive signal cascade (Hardie, 2014; Saxton and Sabatini, 2017). However, our results showed that AMPK is not involved in S6K1 suppression in gastric cancer cells treated with ITV CM (Figure S7B). Thus, we examined mTORC1 activation to investigate the pathway involved in S6K1 suppression by ITV under acidic conditions. As the localization of mTORC1 on the lysosome is a key event for its activation (Son et al., 2019), we analyzed the co-localization of mTOR and LAMP1, a lysosome surface marker, in gastric cancer cells treated with ITV under acidic conditions, ITV/acidic conditions, and ITV CM. Signal overlap of mTOR and LAMP1 was found at ITV, low pH, pH/acidic, and ITV CM except for EBSS, indicating that the suppression of S6K1 phosphorylation is mTORC1 activation independent (Figure S7D).

Sacco et al. (2016) reported that metformin treatment induces protein phosphatase-2A (PP2A)-dependent S6K1 inactivation via undetermined signaling. Thus, we further investigated the effect of PP2A on S6K1 phosphorylation in gastric cancer cells treated with acidic-potentiated ITV. Suppression of S6K1 phosphorylation by ITV CM or pH/ITV treatment was suppressed by calyculin A, an inhibitor of PP2A, and pH neutralization (Figure 4A). In addition, the complete suppression of S6K1 phosphorylation in gastric cancer cells

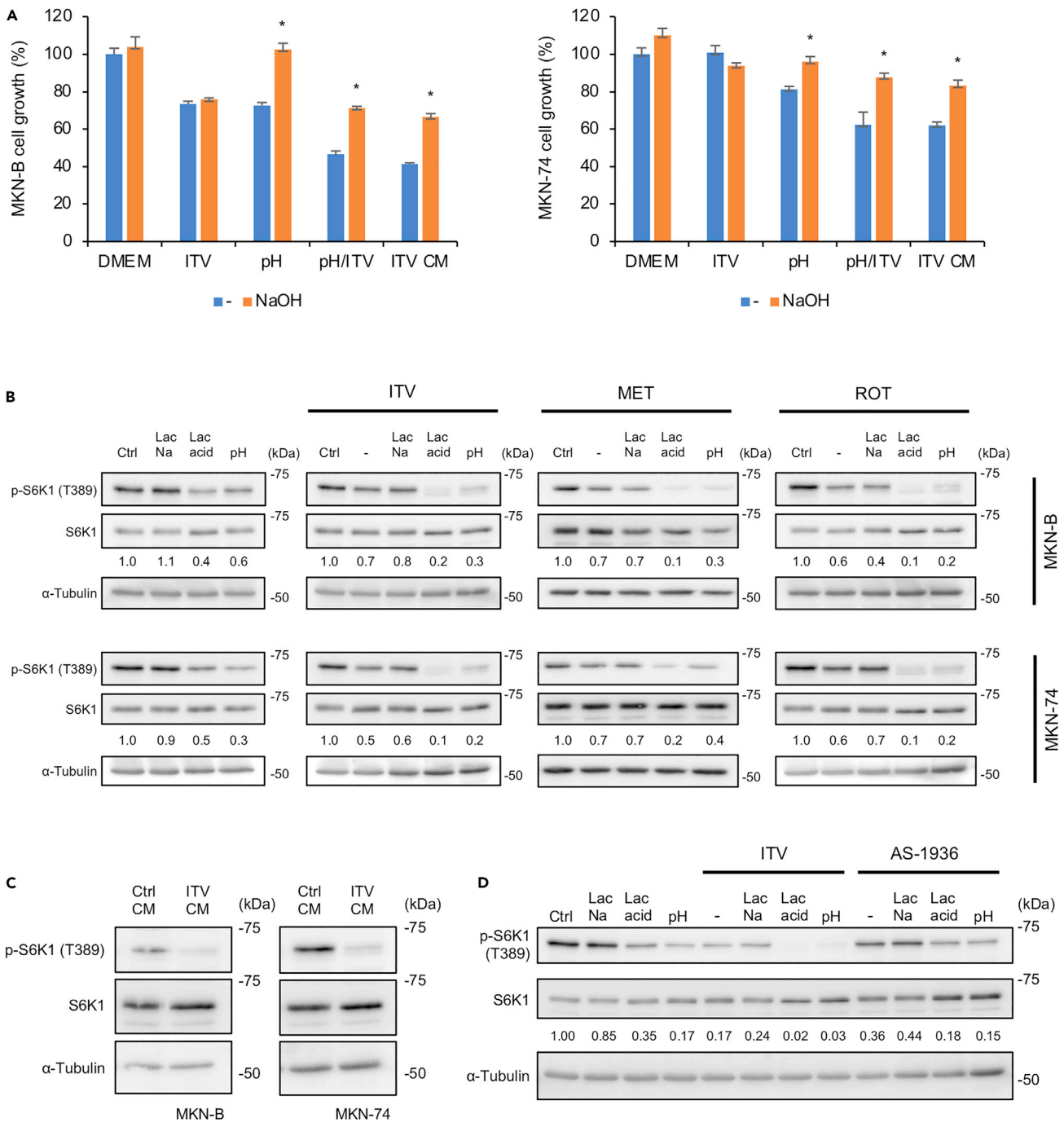

Figure 3. Complex I inhibition and low extracellular pH synergistically suppress S6K1

(A) MTT assay results showing the growth of MKN-B and MKN-74 cells cultured with intervenolin (ITV; 1 μg/mL), low pH medium (pH), low pH medium with ITV (1 μg/mL) (pH/ITV), or ITV CM. Cell viability grown at DMEM without NaOH was defined as 100% (n = 3; *p < 0.05).

(B–D) Western blot analysis showing the phosphorylation levels of S6K1 (T389) in cancer cells with the following culture conditions: (B and D) MKN-B and MKN-74 cells treated with ITV (1 μg/mL), metformin (MET, 1 mg/mL), rotenone (ROT, 0.01 μg/mL), or AS-1936 (1 μg/mL) in DMEM supplemented 1% D-FBS (–), 10 mM sodium lactate (Lac Na), 10 mM lactic acid (Lac acid), or low pH medium (pH) for 3 h. Relative intensities of phospho-S6K1/total S6K1 ratio (versus ctrl) were analyzed by ImageJ and shown. (C) MKN-B and MKN-74 cells cultured in Ctrl CM or ITV CM for 3 h. Data were analyzed using two-sided Student's t test.

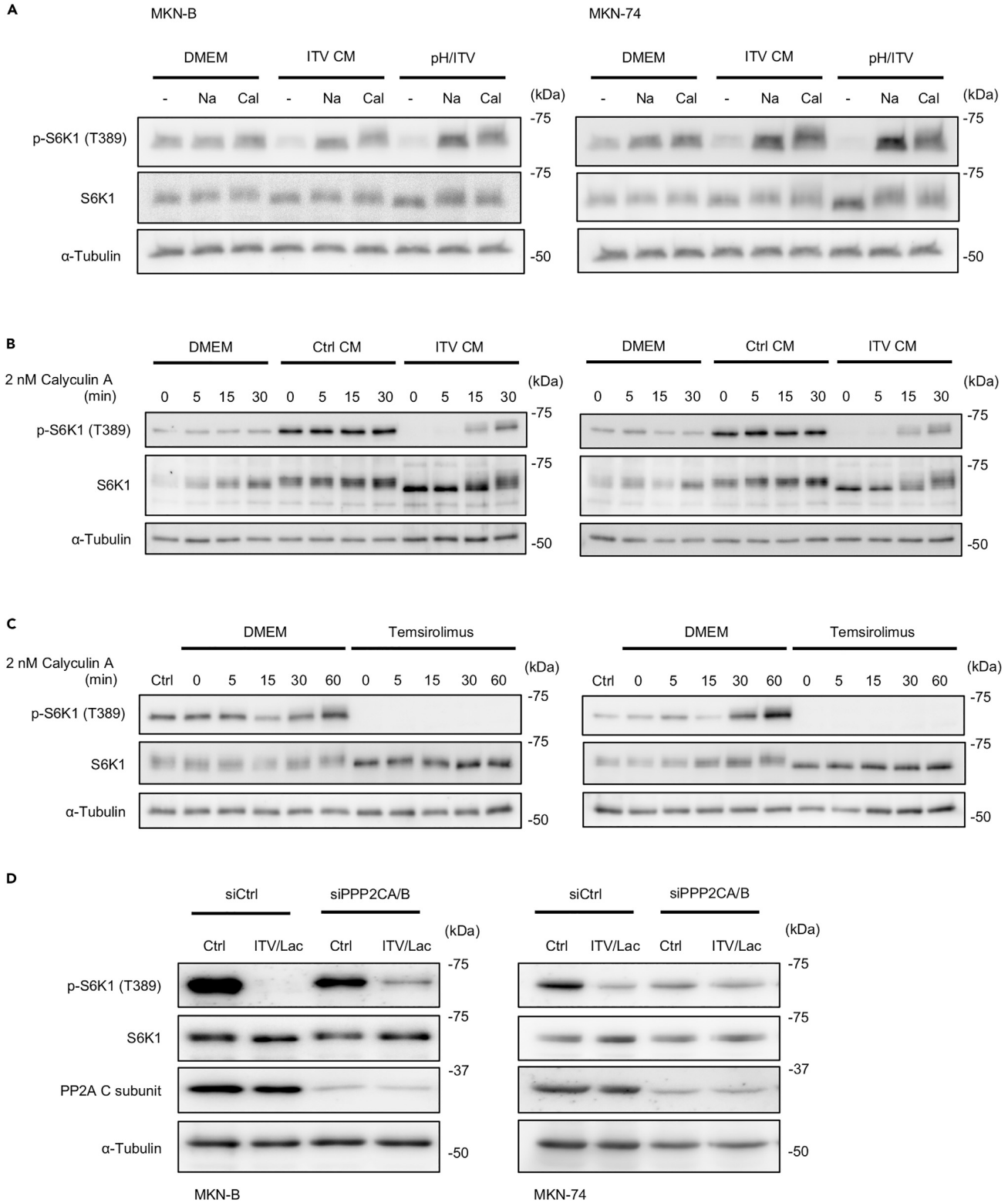

Figure 4. Suppression of S6K1 by intervenolin (ITV) under acidic conditions is dependent on PP2A

(A–D) Western blot analysis showing the phosphorylation levels of S6K1 (T389) in cancer cells with the following culture conditions: (A) MKN-B and MKN-74 cells cultured in DMEM supplemented with 1% D-FBS (DMEM), ITV CM, or low-pH medium containing ITV (1 μg/mL) (pH/ITV) for 3 h and added with NaOH

Figure 4. *Continued*

(Na, 0.1 mM) or calyculin A (Cal, 2 nM) for further 30 min incubation; (B and C) MKN-B and MKN-74 cells cultured in DMEM supplemented 1% D-FBS (DMEM), Ctrl CM, ITV CM, or temsirolimus (25 μM) and added with calyculin A (2 nM) for the indicated time; (D) MKN-B and MKN-74 cells treated with non-target siRNA (siCtrl) or siRNA for *PPP2CA* and *PPP2CB* (PPP2CA/B) and cultured in DMEM supplemented 1% D-FBS (Ctrl) or the medium containing 10 mM lactate and ITV (1 μg/mL; ITV/Lac) for 3 h.

due to ITV CM was recovered by calyculin A as early as 30 min (Figure 4B). In contrast, calyculin A treatment did not restore S6K1 phosphorylated levels after temsirolimus, an mTOR inhibitor, completely suppressed S6K1 phosphorylation (Figure 4C). Moreover, silencing both *PPP2CA* and *PPP2CB* (*PPP2CA/B*), genes encoding for the catalytic subunits of PP2A, in gastric cancer cells attenuated the suppression of S6K1 phosphorylation by ITV at low pH (Figure 4D). These results suggest that the suppression of S6K1 phosphorylation by ITV at low pH is caused by PP2A dephosphorylation.

Proton-sensing G protein-coupled receptor regulates S6K1 suppression by ITV under acidic conditions

GPR4, GPR65 (TDAG8), GPR68 (OGR-1), and GPR132 (G2A) are proton-sensing G protein-coupled receptors (GPCRs) activated by extracellular acidic pH (Chen et al., 2011; Huang et al., 2016; Ihara et al., 2010; Murakami et al., 2004; Saxena et al., 2012). Therefore, we examined whether these GPCRs are involved in S6K1 suppression by complex I inhibitors under acidic conditions. We detected the expression of GPR68 and GPR132, but not GPR4 and GPR65, in MKN-B and MKN-74 cells (Figure 5A). Although ITV significantly inhibited parental cell growth when co-cultured with gastric stromal cells, its inhibitory effect was canceled in *GPR132*-knockout cells (Figures 5B and 5C). Consistent with this, S6K1 phosphorylation in *GPR132*-knockout cells was not suppressed by ITV under acidic conditions induced by lactate (Figure 5D).

Proton-sensing GPCRs are fully activated at pH levels between 6.4 and 6.8 (Ludwig et al., 2003). Here, the pH values used in co-culture experiments were from 6.8 to 6.9. Thus, the results indicate that ITV treatment under acidic conditions suppresses gastric cancer cell growth through GPCRs, particularly GPR132.

Intracellular acidification is crucial for the suppressive activity of ITV under acidic conditions

Because PP2A dephosphorylated S6K1 in gastric cancer cells treated with ITV under acidic conditions, we next explored the related events induced by ITV that act synergistically with low extracellular pH to suppress S6K1. As large amounts of lactate are produced by complex I inhibition, we hypothesized that lactate also accumulates in the cytosol of cancer cells, altering intracellular pH. Following treatment with ITV or nigercin, an H+ and K+ ionophore that lowers intracellular pH, the intracellular pH of MKN-B and MKN-74 cells significantly decreased compared with that of control cells (Figures 5E and 5F). Furthermore, S6K1 phosphorylation in gastric cancer cells was suppressed by nigericin under acidic conditions induced by 10 mM lactate like complex I inhibitors (Figure 5G). These results suggest that reduced intracellular pH due to lactate accumulation acts synergistically with low extracellular pH to suppress S6K1.

Complex I inhibitors suppress S6K1 activity in a mouse xenograft model

To confirm the mode of action of ITV *in vivo*, we performed immunohistochemistry using tumor tissues from MKN-74-bearing mice. We evaluated the phosphorylation of S6K1 and ribosomal protein S6 (RPS6), a substrate of S6K1. As expected, S6K1 and RPS6 phosphorylation levels were decreased by ITV (Figures 6A and 6D). Rotenone and metformin (albeit weakly) similarly suppressed S6K1 and RPS6 phosphorylation (Figures 6B–6D). Although rotenone (0.4 mg/kg) exhibited stronger activity than did ITV, this concentration was toxic for mice. Meanwhile, AMPK phosphorylation levels in tumor tissues remained unchanged after ITV, rotenone, and metformin treatment (Figures 6A–6C).

In addition, ITV, rotenone, and metformin increased lactate levels in tumor tissues (Figure 6E). Of importance, phospho-S6K1 intensity and lactate level in tumor tissues were inversely correlated ($r = -0.57$; Figure 6F). These results indicate that the suppression of S6K1 phosphorylation in tumor tissues occurs in the TME under high lactate concentrations.

ITV exhibits anti-tumor activity in a human pancreatic cancer patient-derived xenograft mouse model

Pancreatic tumor tissues include a significant number of stromal components (von Ahrens et al., 2017). We next examined the anti-cancer activity of ITV and ASP4132, a complex I inhibitor, against pancreatic cancer

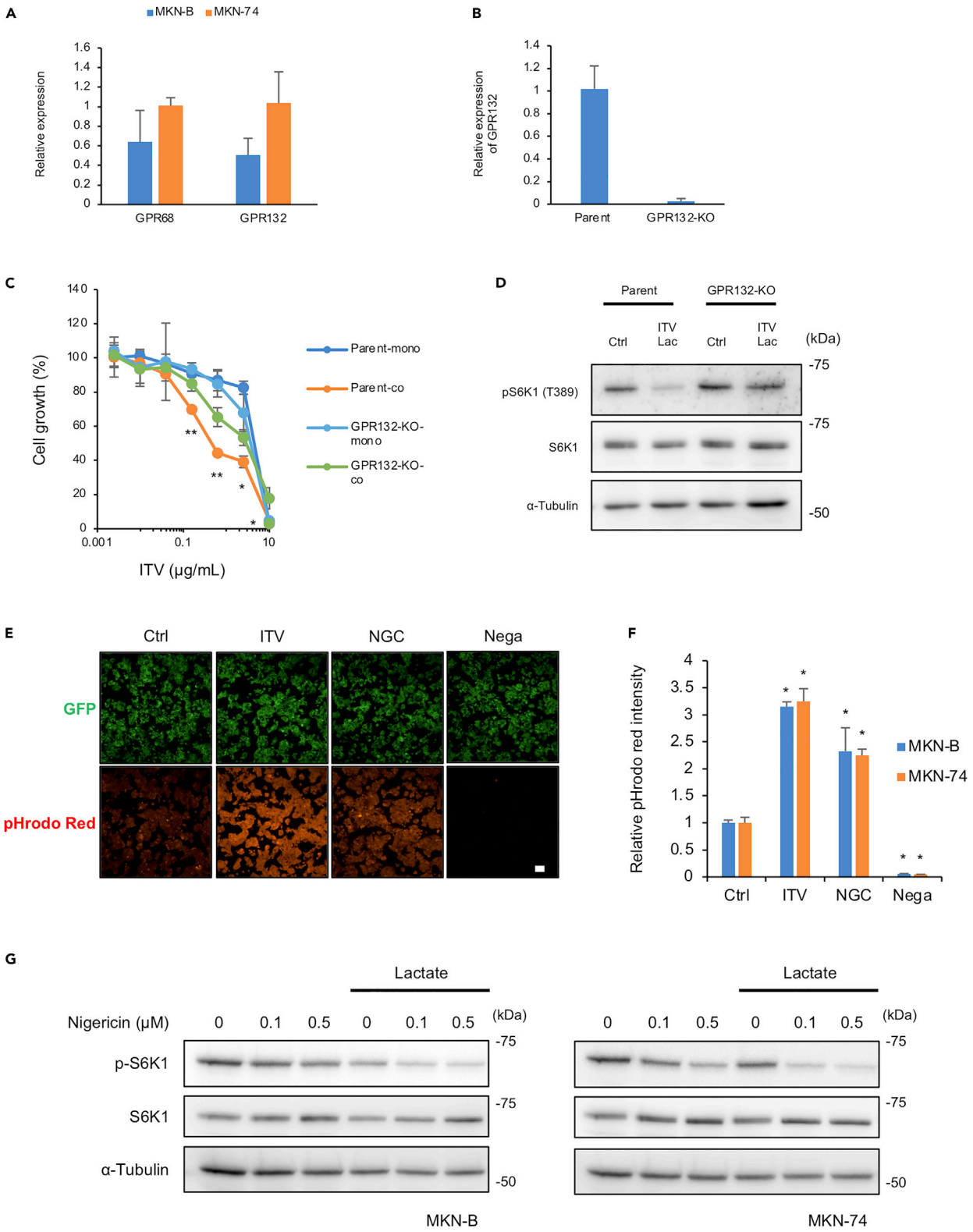

Figure 5. GPR132 is important for intervenolin (ITV) activity, and complex I inhibition leads to intracellular acidification

(A) Relative mRNA expression levels of GPR68 and GPR132 in MKN-B and MKN-74 (versus MKN-74) as measured using qPCR (n = 3).

(B) Relative mRNA expression levels of GPR132 in MKN-74 parent cells (parent) and *GPR132*-knockout cells (*GPR132*-KO).

Figure 5. *Continued*

(C) Parent and *GPR132*-KO cells were cultured alone (Mono) or with Hs738 (Co) for 3 days with the indicated concentrations of ITV. Cell growth was determined by measuring GFP fluorescence intensity (n = 3; *p < 0.05, **p < 0.005 versus mono).

(D) Parent and *GPR132*-KO cells were cultured in the medium containing 8 mM lactate with the indicated concentrations of ITV for 1 h. Western blot analysis shows the phosphorylation levels of S6K1 (T389) in cancer cells.

(E and F) Intracellular pH levels of cancer cells measured using pHrodo Red fluorescence intensity normalized to that of GFP. MKN-B and MKN-74 cells were treated with 1 μg/mL ITV or 0.1 μg/mL nigericin (NGC) for 3 h. Cells not treated with pHrodo Red served as the negative control group (Nega). Scale bar, 100 μm (n = 3; *p < 0.005 versus ctrl).

(G) MKN-B and MKN-74 cells cultured in the medium containing 10 mM lactate with the indicated concentrations of nigericin for 3 h. Western blot analysis shows phosphorylation levels of S6K1 (T389) in cancer cells.

Data are presented as the mean ± SD and were analyzed using two-sided Student's t test.

cells. Both ITV and ASP4132 significantly suppressed the growth of pancreatic cancer cells co-cultured with pancreatic normal stellate cells HPaSteC at lower concentrations than in monocultures (Figure S8A). *In vitro* evaluation showed that ASP4132 more strongly inhibited complex I activity and gastric cancer cell growth upon co-culture than did ITV (Figures S8B and S8C). As expected, both ASP4132-treated CM from Hs738 cells and ITV-treated CM suppressed S6K1 phosphorylation (Figure S8D). In addition, ASP4132 significantly inhibited BxPC-3 xenograft growth without any body weight loss and reduced RSP6 phosphorylation in tumor tissues (Figures S9A and S9B).

Finally, we examined the anti-tumor activity of ITV using a human pancreatic cancer PDX model. ITV-treated mice showed significantly inhibited tumor growth on days 10 (P = 0.016), 14 (P = 0.023), and 17 (P = 0.009) compared with vehicle-treated mice without any body weight loss (Figures 7A and 7B). Moreover, ITV significantly reduced phosphorylated RSP6 levels and BrdU-positive cell number (Figures 7C–7F). These results indicate that ITV shows potent anti-tumor activity against human pancreatic cancer PDX models and exhibits the same mode of action *in vivo*.

DISCUSSION

In normal cells, OXPHOS is the main metabolic pathway that generates energy, producing ATP through the ETC, which comprises mitochondrial complexes I, II, III, IV, and ATP-synthase (complex V). Energy produced via OXPHOS is driven by the electron donors NADH and FADH2 generated by the TCA cycle and ATP produced in complex V via the proton gradient between the inner membrane space and mitochondrial matrix. As the first step of the ETC, the proton gradient is generated via the proton pump function of complexes I and II, but mainly complex I. Therefore, complex I is a target molecule for inhibiting OXPHOS in chemotherapy.

In cancer cells, glycolysis is facilitated by the Warburg effect, which is a hallmark feature of all cancers, and OXPHOS is suppressed (Balsa et al., 2020; Koppenol et al., 2011; Zhang et al., 2020). However, several human tumors such as glioblastoma and leukemia mainly depend on OXPHOS and not glycolysis for energy generation, leading to the formation of a hypoxic TME, which can be exploited for cancer therapy (DeBerardinis and Chandel, 2020; Hensley et al., 2016; Kennedy et al., 2013). Therefore, energy depletion induced by OXPHOS inhibition is a promising strategy for the treatment of such cancers.

Here, we analyzed the mechanism of action of the natural compound ITV and revealed anti-tumor strategy that is independent of energy depletion. Complex I inhibitors shifted the metabolism from OXPHOS to glycolysis, resulting in the production of lactate in cancer cells, similar to the Warburg effect. Extracellular pH decreases due to excess lactate, and intracellular pH also decreases due to the accumulation of intracellular lactate. Intra- and extracellular acidification works synergistically to suppress S6K1 phosphorylation through PP2A. Proton-sensing GPCRs are fully active at a pH of ~6.8, which is consistent with the pH of the ITV CM and the acidic conditions used in this study. The reduction in pH was sensed by proton-sensing GPCRs, whereas the growth suppressive activity of ITV under acidic conditions was partially attenuated in *GPR132*-knockout cells. Hence, GPR132 plays an important role in pH sensing to suppress S6K1 through PP2A (Figure 7G). The regulation of PP2A through activated GPCRs is functionally regulated by protein kinase A by increasing intracellular cAMP levels (Faubert et al., 2017; Leslie and Nairn, 2019). The regulation of the substrate specificity of PP2A is complicated. PP2A is a heterotrimer consisting of a scaffolding subunit A, catalytic subunit C, and regulatory subunit B; because each subunit has numerous isoforms (subunit A: 2, subunit C: 2, subunit B: at least 16 types in combination), many isoform combinations of PP2A exist, and the composition of each subunit determines substrate specificity (Ahn et al., 2007; DeGrande et al.,

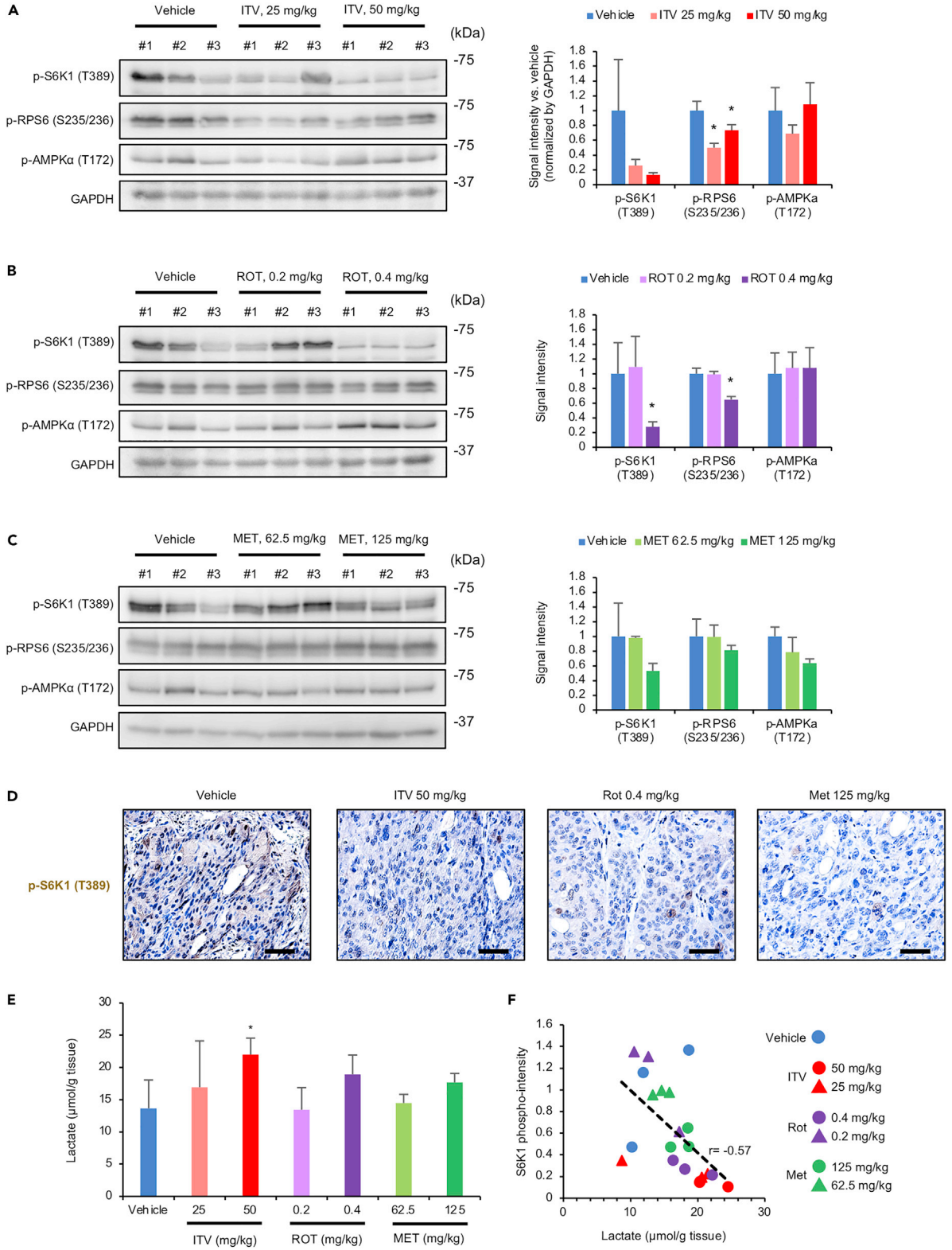
A
Vehicle
ITV, 25 mg/kg
ITV, 50 mg/kg
(kDa)
#1 #2 #3 #1 #2 #3 #1 #2 #3
p-S6K1 (T389)
p-RPS6 (S235/236)
p-AMPKα (T172)
GAPDH
-75
-75
-75
-37
Vehicle
ITV 25 mg/kg
ITV 50 mg/kg
Signal intensity vs. vehicle (normalized by GAPDH)
p-S6K1 (T389)
p-RPS6 (S235/236)
p-AMPKa (T172)
B
Vehicle
ROT, 0.2 mg/kg
ROT, 0.4 mg/kg
Signal intensity
C
Vehicle
MET, 62.5 mg/kg
MET, 125 mg/kg
D
Vehicle
ITV 50 mg/kg
Rot 0.4 mg/kg
Met 125 mg/kg
p-S6K1 (T389)
E
Lactate (μmol/g tissue)
Vehicle
25
50
0.2
0.4
62.5
125
ITV (mg/kg)
ROT (mg/kg)
MET (mg/kg)
F
S6K1 phospho-intensity
r= -0.57
Lactate (μmol/g tissue)
Vehicle
ITV
50 mg/kg
25 mg/kg
Rot
0.4 mg/kg
0.2 mg/kg
Met
125 mg/kg
62.5 mg/kg

Figure 6. Intervenolin (ITV) suppresses intratumor S6K1 phosphorylation and elevates intratumor lactate levels in MKN-74-inoculated mouse xenograft models

(A–C) Western blot analysis showing the phosphorylation levels of S6K1 (T389), RPS6 (S235/236), and AMPK (T172) in tumor tissues from mice treated with ITV, rotenone (ROT), or metformin (MET) at the indicated doses. Signal intensities of the bands are shown in the bar graph ($n = 3$; *$p < 0.005$ versus vehicle).

(D) Formalin-fixed, paraffin-embedded tumor sections from mice treated with the vehicle, ITV, ROT, or MET were analyzed by immunohistochemistry using antibodies against phospho-S6K1 (T389). Scale bar, 100 μm ($n = 3$).

(E) Lactate levels in tumor tissues from mice treated with the vehicle, ITV, ROT, or MET ($n = 3$; *$p < 0.005$ versus vehicle).

(F) S6K1 phosphorylation and lactate levels in tumor tissues from mice treated with the vehicle, ITV, ROT, or MET are significantly inversely correlated. r represents Pearson's correlation coefficient.

Data are presented as the mean ± SD and were analyzed using two-sided Student's t test.

2013). Although the complete suppression of S6K1 requires intracellular acidification in addition to pH sensing by PP2A, the mechanism of PP2A regulation in response to acidification remains unclear and requires further investigation.

The pH inside solid tumors is extremely low (~pH 6) owing to increased lactic acid produced by the Warburg effect. In our experiments, we found that complex I inhibition can further enhance glycolysis even inside cancer cells and that lactate secretion can be also further enhanced even in tumor tissues. Although the extracellular pH in tumor tissues is lower than in normal tissue, the intracellular pH in both tumor tissues and normal tissues was maintained (Webb et al., 2011). Although the extent of its activity could be possibly altered depending on expression levels of proton pumps and monocarboxylate transporters in cancer cells, anti-tumor activity via the concomitant acidification of both the intra- and extracellular environment through the inhibition of complex I is expected to be effective against solid tumors. Moreover, TMEs originally exhibiting a low pH are good targets for our proposed strategy using complex I inhibitors.

Unlike cancer cells, the energy production in stromal cells, such as Hs738 cells, depends on OXPHOS; thus, the magnitude of TME acidification induced by complex I inhibition in the presence of stromal cells markedly exceeded that of cancer cells alone. Therefore, the strategy of concomitant intra- and extra acidification induced by complex I inhibitors is more effective against solid tumors harboring abundant stromal cells. A strong stromal reaction is a hallmark of pancreatic ductal adenocarcinoma (PDAC). PDAC is the most common pancreatic cancer type and has the lowest overall survival rate of approximately 8% (Siegel et al., 2019). Patients with PDAC show poor response to chemotherapy and immune checkpoint inhibition therapy (Kabacaoglu et al., 2018). Therefore, the development of a more effective PDAC therapy is urgently needed. We found that ITV suppressed gastric cancer cell growth in both mouse xenograft models and human pancreatic cancer PDX models. Because ITV treatment under acidic conditions induced the death of gastric cancer cells (Figure S9C), the concomitant intra- and extra acidification strategy using complex I inhibitors is a promising therapeutic strategy for intractable cancers. This mechanism of action of complex I inhibitors against solid tumors can be used as a new anti-cancer strategy and for drug development.

In our *in vitro* experiments, rotenone, a well-known complex I inhibitor, strongly exhibited adverse toxicity, whereas metformin had a weak effect on tumor growth. Rotenone also inhibits myotube formation, which can have neurotoxic effects (Liu et al., 2005; Zhang et al., 2019). The limitations of metformin for cancer treatment, including inadequate potency and transport-mediated accumulation, have been previously reported (Wang et al., 2002). Although rotenone and metformin have similar *in vitro* inhibitory activity as ITV, we demonstrated that ITV is the best anti-cancer agent among these compounds. Indeed, ITV-treated mice did not show any weight loss even at the tumor-suppressive dose. Currently, we are synthesizing several derivatives of ITV that exhibit anti-tumor effects via complex I activity inhibition (Figure S9D, Table S2). Overall, our findings help contribute to the development of efficacious anti-cancer drugs.

Limitations of the study

Our current study demonstrated that anti-tumor activity via the concomitant acidification of both the intra- and extracellular environment through the inhibition of complex I could be applied to solid tumors. Since many types of transporters and proton pumps are involved in pH maintenance of cancer cells, it can be considered that the expression levels and genetic mutations of these factors could possibly alter the anti-tumor activity of complex I inhibitors. The extracellular acidification induced by complex I inhibitor is dependent on the activity of lactate transporters. Even if cancer cells have lower lactate transporter activity, cancer cells surrounding stromal cells could secrete lactate and induce extracellular acidification by

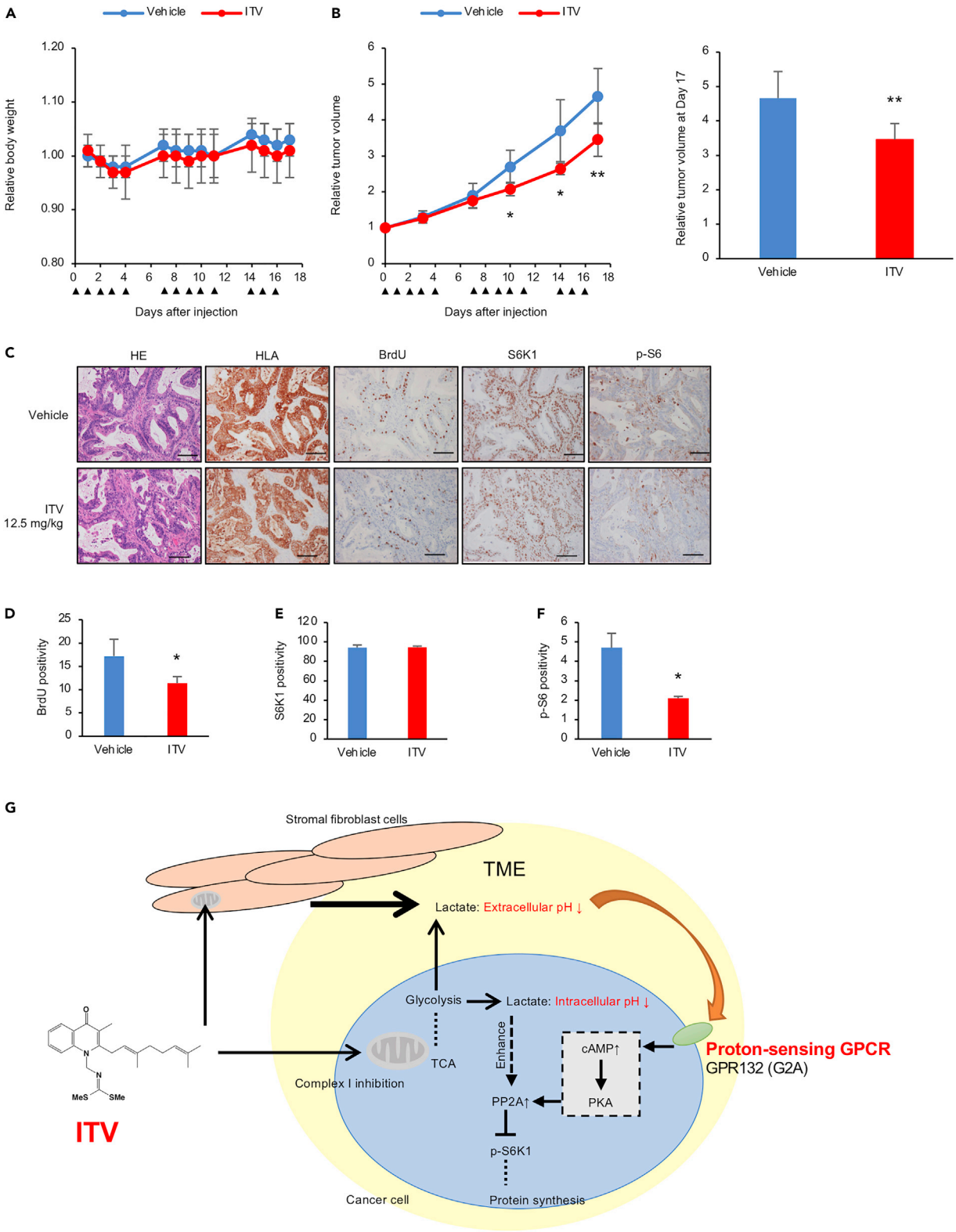

Figure 7. Intervenolin (ITV) suppresses tumor growth in mouse PDX models

(A) Mice treated with ITV (12.5 mg/kg; $n = 6$) did not show any weight loss compared with those with the vehicle ($n = 7$).

(B) Relative tumor volumes (*$p < 0.005$, **$p < 0.01$ versus vehicle) at 17 days from ITV injection. ITV was injected on the days indicated by black triangles.

Figure 7. *Continued*
(C) Immunohistochemistry analysis of tumor sections from mice treated with the vehicle or ITV. Scale bar, 100 μm.
(D–F) Percentages of BrdU-, S6K1-, and p-S6-positive cells in the tumor sections (*$p < 0.05$).
(G) Proposed mechanism of ITV anti-cancer activity.
Data are presented as the mean ± SD and were analyzed using two-sided Student's t test.

complex I inhibitors. On the other hand, the intracellular acidification can be modified due to the activity of intracellular pH-maintenance factors.

We confirmed the anti-tumor activity of ITV through S6K1 suppression using a PDX model reproducing the heterogeneity of cancer cells of a patient origin, but it should be noted that we used only one PDX model derived from a single patient.

STAR★METHODS

Detailed methods are provided in the online version of this paper and include the following:

- KEY RESOURCES TABLE
- RESOURCE AVAILABILITY
  - Lead contact
  - Materials availability
  - Data and code availability
- EXPERIMENTAL MODEL AND SUBJECT DETAILS
  - Animals
- METHOD DETAILS
  - Reagents
  - Cell viability assays
  - Mouse xenograft models
  - Isolation of mouse fibroblasts
  - OCR and extracellular acidification
  - Enzymatic activity of complex I
  - Pull-down assay
  - Measurement of lactate and glucose levels
  - Metabolite extraction and metabolomic analysis
  - Western blot analysis
  - siRNA transfection
  - Immunofluorescence
  - Gene knockout
  - Quantitative PCR
  - Intracellular pH
  - Sample preparation from mouse tumor tissues
  - Histology and immunohistochemistry
  - BrdU labeling assay
  - PDX model
  - Flow cytometry
- QUANTIFICATION AND STATISTICAL ANALYSIS

SUPPLEMENTAL INFORMATION

Supplemental information can be found online at https://doi.org/10.1016/j.isci.2021.103497.

ACKNOWLEDGMENTS

The authors thank Dr. Isao Momose, Dr. Daisuke Tatsuda, Dr. Shun-ichi Wada, Dr. Tomoko Nakanishi, and Ms. Akiko Harakawa (BIKAKEN); Dr. Ken Matsumoto, Dr. Yoko Yashiroda, and Dr. Minoru Yoshida (RIKEN); and Ms. Kanami Yamazaki, Dr. Tetsuo Mashima, and Dr. Akihiro Tomida (JFCR) for their fruitful suggestions and technical support. This work was supported in part by the Molecular Profiling Committee; Grant-in-Aid for Scientific Research on Innovative Areas "Advanced Animal Model Support (AdAMS)" from The Ministry of Education, Culture, Sports, Science and Technology, Japan (MEXT) (JSPS KAKENHI grant number JP 16H06276); the Project for Cancer Research and Therapeutic Evolution (P-CREATE) of the Japan Agency

for Medical Research and Development (grant numbers JP20cm010623h to M.K. and JP20cm0106002h to Y.K.); Grant-in-Aid for Scientific Research (grant number 18K05366); and a Grant-in-Aid for Scientific Research on Innovative Areas (grant number 18H05503 to Y.K.) from MEXT.

AUTHOR CONTRIBUTIONS

J.Y. designed and performed most *in vitro* experiments, analyzed the data, and wrote the manuscript. T.O., S.O., and H.I. performed *in vivo* experiments with mouse xenograft models. H.A., R.O., C.S., and T.W. synthesized ITV and its derivatives. I.U. and M.A. performed some of the co-culture experiments using ITV derivatives and provided technical assistance. S.D. predicted the mode of action of ITV using JFCR39. M. Sugawara., T.K., J.U., Y.A., A.I., M.T., G.A., and T.N. established the PDX models. Y.K., K.H., and H.O. Prepared the compound-conjugate beads. T.S. and M. Shibasaki. supervised and edited the manuscript. M.K. supervised the work and wrote the manuscript.

DECLARATION OF INTERESTS

The authors declare no competing interests.

Received: September 7, 2021
Revised: October 25, 2021
Accepted: November 19, 2021
Published: December 17, 2021

REFERENCES

Abe, H., Kawada, M., Inoue, H., Ohba, S., Nomoto, A., Watanabe, T., and Shibasaki, M. (2013a). Synthesis of intervenolin, an antitumor natural quinolone with unusual substituents. Org. Lett. *15*, 2124–2127.

Abe, H., Kawada, M., Inoue, H., Ohba, S., Masuda, T., Hayashi, C., Igarashi, M., Nomoto, A., Watanabe, T., and Shibasaki, M. (2013b). Structure-activity relationship study of intervenolin derivatives: synthesis, antitumor, and anti-*Helicobacter pylori* activities. Tetrahedron *69*, 7608–7617.

Ahn, J.H., McAvoy, T., Rakhilin, S.V., Nishi, A., Greengard, P., and Nairn, A.C. (2007). Protein kinase A activates protein phosphatase 2A by phosphorylation of the B56delta subunit. Proc. Natl. Acad. Sci. U S A *104*, 2979–2984.

Ashton, T.M., McKenna, W.G., Kunz-Schughart, L.A., and Higgins, G.S. (2018). Oxidative phosphorylation as an emerging target in cancer therapy. Clin. Cancer Res. *24*, 2482–2490.

Balsa, E., Perry, E.A., Bennett, C.F., Jedrychowski, M., Gygi, S.P., Doench, J.G., and Puigserver, P. (2020). Defective NADPH production in mitochondrial disease complex I causes inflammation and cell death. Nat. Commun. *11*, 2714.

Bridges, H.R., Jones, A.J., Pollak, M.N., and Hirst, J. (2014). Effects of metformin and other biguanides on oxidative phosphorylation in mitochondria. Biochem. J. *462*, 475–487.

Chen, A., Dong, L., Leffler, N.R., Asch, A.S., Witte, O.N., and Yang, L.V. (2011). Activation of GPR4 by acidosis increases endothelial cell adhesion through the cAMP/Epac pathway. PLoS One *6*, e27586.

Dan, S., Tsunoda, T., Kitahara, O., Yanagawa, R., Zembutsu, H., Katagiri, T., Yamazaki, K., Nakamura, Y., and Yamori, T. (2002). An integrated database of chemosensitivity to 55 anticancer drugs and gene expression profiles of 39 human cancer cell lines. Cancer Res. *62*, 1139–1147.

DeBerardinis, R.J., and Chandel, N.S. (2020). We need to talk about the Warburg effect. Nat. Metab. *2*, 127–129.

DeGrande, S.T., Little, S.C., Nixon, D.J., Wright, P., Snyder, J., Dun, W., Murphy, N., Kilic, A., Higgins, R., Binkley, P.F., et al. (2013). Molecular mechanisms underlying cardiac protein phosphatase 2A regulation in heart. J. Biol. Chem. *288*, 1032–1046.

Eckert, M.A., Coscia, F., Chryplewicz, A., Chang, J.W., Hernandez, K.M., Pan, S., Tienda, S.M., Nahotko, D.A., Li, G., Blaženović, I., et al. (2019). Proteomics reveals NNMT as a master metabolic regulator of cancer-associated fibroblasts. Nature *569*, 723–728.

Ehinger, J.K., Piel, S., Ford, R., Karlsson, M., Sjövall, F., Frostner, E., Morota, S., Taylor, R.W., Turnbull, D.M., Cornell, C., et al. (2016). Cell-permeable succinate prodrugs bypass mitochondrial complex I deficiency. Nat. Commun. *7*, 12317.

Erez, N., Truitt, M., Olson, P., Arron, S.T., and Hanahan, D. (2010). Cancer-associated fibroblasts are activated in incipient neoplasia to orchestrate tumor-promoting inflammation in an NF-kappaB-Dependent manner. Cancer Cell *17*, 135–147.

Faubert, B., Li, K.Y., Cai, L., Hensley, C.T., Kim, J., Zacharias, L.G., Yang, C., Do, Q.N., Doucette, S., Burguete, D., et al. (2017). Lactate metabolism in human lung tumors. Cell *171*, 358–371.e359.

Hao, J., Yan, F., Zhang, Y., Triplett, A., Zhang, Y., Schultz, D.A., Sun, Y., Zeng, J., Silverstein, K.A.T., Zheng, Q., et al. (2018). Expression of adipocyte/macrophage fatty acid-binding protein in tumor-associated macrophages promotes breast cancer progression. Cancer Res. *78*, 2343–2355.

Hardie, D.G. (2014). AMPK–sensing energy while talking to other signaling pathways. Cell Metab. *20*, 939–952.

Hensley, C.T., Faubert, B., Yuan, Q., Lev-Cohain, N., Jin, E., Kim, J., Jiang, L., Ko, B., Skelton, R., Loudat, L., et al. (2016). Metabolic heterogeneity in human lung tumors. Cell *164*, 681–694.

Hida, K., Hida, Y., Amin, D.N., Flint, A.F., Panigrahy, D., Morton, C.C., and Klagsbrun, M. (2004). Tumor-associated endothelial cells with cytogenetic abnormalities. Cancer Res. *64*, 8249–8255.

Huang, Y.H., Su, Y.S., Chang, C.J., and Sun, W.H. (2016). Heteromerization of G2A and OGR1 enhances proton sensitivity and proton-induced calcium signals. J. Receptor Signal Transduction Res. *36*, 633–644.

Huang, Z., Zhang, M., Chen, G., Wang, W., Zhang, P., Yue, Y., Guan, Z., Wang, X., and Fan, J. (2019). Bladder cancer cells interact with vascular endothelial cells triggering EGFR signals to promote tumor progression. Int. J. Oncol. *54*, 1555–1566.

Ihara, Y., Kihara, Y., Hamano, F., Yanagida, K., Morishita, Y., Kunita, A., Yamori, T., Fukayama, M., Aburatani, H., Shimizu, T., et al. (2010). The G protein-coupled receptor T-cell death-associated gene 8 (TDAG8) facilitates tumor development by serving as an extracellular pH sensor. Proc. Natl. Acad. Sci. U S A *107*, 17309–17314.

Junker, B.H., Klukas, C., and Schreiber, F. (2006). VANTED: a system for advanced data analysis and visualization in the context of biological networks. BMC Bioinformatics *7*, 109.

Kabacaoglu, D., Ciecielski, K.J., Ruess, D.A., and Algül, H. (2018). Immune checkpoint inhibition for pancreatic ductal adenocarcinoma: current limitations and future options. Front. Immunol. *9*, 1878.

Kalender, A., Selvaraj, A., Kim, S.Y., Gulati, P., Brûlé, S., Viollet, B., Kemp, B.E., Bardeesy, N., Dennis, P., Schlager, J.J., et al. (2010). Metformin, independent of AMPK, inhibits mTORC1 in a rag GTPase-dependent manner. Cell Metab. *11*, 390–401.

Kalluri, R. (2016). The biology and function of fibroblasts in cancer. Nat. Rev. Cancer *16*, 582–598.

Kanoh, N., Honda, K., Simizu, S., Muroi, M., and Osada, H. (2005). Photo-cross-linked small-molecule affinity matrix for facilitating forward and reverse chemical genetics. Angew. Chem. Int. Ed. Engl. *44*, 3559–3562.

Kawada, M., Inoue, H., Ohba, S., Hatano, M., Amemiya, M., Hayashi, C., Usami, I., Abe, H., Watanabe, T., Kinoshita, N., et al. (2013). Intervenolin, a new antitumor compound with anti-Helicobacter pylori activity, from Nocardia sp. ML96-86F2. J. Antibiot. *66*, 543–548.

Kawada, M., Inoue, H., Ohba, S., Masuda, T., Momose, I., and Ikeda, D. (2010a). Leucinostatin A inhibits prostate cancer growth through reduction of insulin-like growth factor-I expression in prostate stromal cells. Int. J. Cancer *126*, 810–818.

Kawada, M., Inoue, H., Ohba, S., Yoshida, J., Masuda, T., Yamasaki, M., Usami, I., Sakamoto, S., Abe, H., Watanabe, T., et al. (2015). Stromal cells positively and negatively modulate the growth of cancer cells: stimulation via the PGE2-TNFα-IL-6 pathway and inhibition via secreted GAPDH-E-cadherin interaction. PLoS One *10*, e0119415.

Kawada, M., Inoue, H., Usami, I., and Ikeda, D. (2009a). Phthoxazolin A inhibits prostate cancer growth by modulating tumor-stromal cell interactions. Cancer Sci. *100*, 150–157.

Kawada, M., Momose, I., Someno, T., Tsujiuchi, G., and Ikeda, D. (2009b). New atpenins, NBRI23477 A and B, inhibit the growth of human prostate cancer cells. J. Antibiot. *62*, 243–246.

Kawada, M., Someno, T., Inoue, H., Ohba, S., Masuda, T., Kato, T., and Ikeda, D. (2010b). NBRI16716A, a new antitumor compound against human prostate cancer cells, produced by Perisporiopsis melioloides Mer-f16716. J. Antibiot. *63*, 319–323.

Kennedy, K.M., Scarbrough, P.M., Ribeiro, A., Richardson, R., Yuan, H., Sonveaux, P., Landon, C.D., Chi, J.T., Pizzo, S., Schroeder, T., et al. (2013). Catabolism of exogenous lactate reveals it as a legitimate metabolic substrate in breast cancer. PLoS One *8*, e75154.

Koppenol, W.H., Bounds, P.L., and Dang, C.V. (2011). Otto Warburg's contributions to current concepts of cancer metabolism. Nat. Rev. Cancer *11*, 325–337.

Kuramoto, K., Yamada, H., Shin, T., Sawada, Y., Azami, H., Yamada, T., Nagashima, T., and Ohnuki, K. (2020). Development of a potent and orally active activator of adenosine monophosphate-activated protein kinase (AMPK), ASP4132, as a clinical candidate for the treatment of human cancer. Bioorg. Med. Chem. *28*, 115307.

Lambrechts, D., Wauters, E., Boeckx, B., Aibar, S., Nittner, D., Burton, O., Bassez, A., Decaluwé, H., Pircher, A., Van den Eynde, K., et al. (2018). Phenotype molding of stromal cells in the lung tumor microenvironment. Nat. Med. *24*, 1277–1289.

Lavin, Y., Kobayashi, S., Leader, A., Amir, E.D., Elefant, N., Bigenwald, C., Remark, R., Sweeney, R., Becker, C.D., Levine, J.H., et al. (2017). Innate immune landscape in early lung adenocarcinoma by paired single-cell analyses. Cell *169*, 750–765.e717.

Leslie, S.N., and Nairn, A.C. (2019). cAMP regulation of protein phosphatases PP1 and PP2A in brain. Biochim. Biophys. Acta Mol. Cel. Res. *1866*, 64–73.

Liu, H.Q., Zhu, X.Z., and Weng, E.Q. (2005). Intracellular dopamine oxidation mediates rotenone-induced apoptosis in PC12 cells. Acta Pharmacol. Sin. *26*, 17–26.

Livak, K.J., and Schmittgen, T.D. (2001). Analysis of relative gene expression data using real-time quantitative PCR and the 2(-Delta Delta C(T)) Method. Methods *25*, 402–408.

Ludwig, M.G., Vanek, M., Guerini, D., Gasser, J.A., Jones, C.E., Junker, U., Hofstetter, H., Wolf, R.M., and Seuwen, K. (2003). Proton-sensing G-protein-coupled receptors. Nature *425*, 93–98.

Mantovani, A., Marchesi, F., Malesci, A., Laghi, L., and Allavena, P. (2017). Tumour-associated macrophages as treatment targets in oncology. Nat. Rev. Clin. Oncol. *14*, 399–416.

Mizutani, Y., Kobayashi, H., Iida, T., Asai, N., Masamune, A., Hara, A., Esaki, N., Ushida, K., Mii, S., Shiraki, Y., et al. (2019). Meflin-positive cancer-associated fibroblasts inhibit pancreatic carcinogenesis. Cancer Res. *79*, 5367–5381.

Molina, J.R., Sun, Y., Protopopova, M., Gera, S., Bandi, M., Bristow, C., McAfoos, T., Morlacchi, P., Ackroyd, J., Agip, A.A., et al. (2018). An inhibitor of oxidative phosphorylation exploits cancer vulnerability. Nat. Med. *24*, 1036–1046.

Murakami, N., Yokomizo, T., Okuno, T., and Shimizu, T. (2004). G2A is a proton-sensing G-protein-coupled receptor antagonized by lysophosphatidylcholine. J. Biol. Chem. *279*, 42484–42491.

Nakatsu, N., Nakamura, T., Yamazaki, K., Sadahiro, S., Makuuchi, H., Kanno, J., and Yamori, T. (2007). Evaluation of action mechanisms of toxic chemicals using JFCR39, a panel of human cancer cell lines. Mol. Pharmacol. *72*, 1171–1180.

Nishiya, N., Oku, Y., Ishikawa, C., Fukuda, T., Dan, S., Mashima, T., Ushijima, M., Furukawa, Y., Sasaki, Y., Otsu, K., et al. (2021). Lamellarin 14, a derivative of marine alkaloids, inhibits the T790M/C797S mutant epidermal growth factor receptor. Cancer Sci. *112*, 1963–1974.

Ohashi, Y., Hirayama, A., Ishikawa, T., Nakamura, S., Shimizu, K., Ueno, Y., Tomita, M., and Soga, T. (2008). Depiction of metabolome changes in histidine-starved Escherichia coli by CE-TOFMS. Mol. bioSystems *4*, 135–147.

Ohishi, T., Masuda, T., Abe, H., Hayashi, C., Adachi, H., Ohba, S.I., Igarashi, M., Watanabe, T., Mimuro, H., Amalia, E., et al. (2018). Monotherapy with a novel intervenolin derivative, AS-1934, is an effective treatment for Helicobacter pylori infection. Helicobacter *23*, e12470.

Ooga, T., Sato, H., Nagashima, A., Sasaki, K., Tomita, M., Soga, T., and Ohashi, Y. (2011). Metabolomic anatomy of an animal model revealing homeostatic imbalances in dyslipidaemia. Mol. bioSystems *7*, 1217–1223.

Paull, K.D., Shoemaker, R.H., Hodes, L., Monks, A., Scudiero, D.A., Rubinstein, L., Plowman, J., and Boyd, M.R. (1989). Display and analysis of patterns of differential activity of drugs against human tumor cell lines: development of mean graph and COMPARE algorithm. J. Natl. Cancer Inst. *81*, 1088–1092.

Pernicova, I., and Korbonits, M. (2014). Metformin–mode of action and clinical implications for diabetes and cancer. Nat. Rev. Endocrinol. *10*, 143–156.

Ravanel, P., Tissut, M., and Douce, R. (1984). Effects of rotenoids on isolated plant mitochondria. Plant Physiol. *75*, 414–420.

Sacco, F., Silvestri, A., Posca, D., Pirrò, S., Gherardini, P.F., Castagnoli, L., Mann, M., and Cesareni, G. (2016). Deep proteomics of breast cancer cells reveals that metformin rewires signaling networks away from a pro-growth state. Cell Syst. *2*, 159–171.

Saxena, H., Deshpande, D.A., Tiegs, B.C., Yan, H., Battafarano, R.J., Burrows, W.M., Damera, G., Panettieri, R.A., Dubose, T.D., Jr., An, S.S., et al. (2012). The GPCR OGR1 (GPR68) mediates diverse signalling and contraction of airway smooth muscle in response to small reductions in extracellular pH. Br. J. Pharmacol. *166*, 981–990.

Saxton, R.A., and Sabatini, D.M. (2017). mTOR signaling in growth, metabolism, and disease. Cell *169*, 361–371.

Siegel, R.L., Miller, K.D., and Jemal, A. (2019). Cancer statistics, 2019. CA: A Cancer J. Clinicians *69*, 7–34.

Son, S.M., Park, S.J., Lee, H., Siddiqi, F., Lee, J.E., Menzies, F.M., and Rubinsztein, D.C. (2019). Leucine signals to mTORC1 via its metabolite acetyl-coenzyme A. Cell Metab. *29*, 192–201.e197.

Sousa, C.M., Biancur, D.E., Wang, X., Halbrook, C.J., Sherman, M.H., Zhang, L., Kremer, D., Hwang, R.F., Witkiewicz, A.K., Ying, H., et al. (2016). Pancreatic stellate cells support tumour metabolism through autophagic alanine secretion. Nature *536*, 479–483.

Spinazzi, M., Casarin, A., Pertegato, V., Salviati, L., and Angelini, C. (2012). Assessment of mitochondrial respiratory chain enzymatic activities on tissues and cultured cells. Nat. Protoc. *7*, 1235–1246.

Sugimoto, M., Wong, D.T., Hirayama, A., Soga, T., and Tomita, M. (2010). Capillary electrophoresis mass spectrometry-based saliva metabolomics identified oral, breast and pancreatic cancer-specific profiles. Metabolomics *6*, 78–95.

Suvarna, K., Honda, K., Muroi, M., Kondoh, Y., Watanabe, N., and Osada, H. (2020). Identification of target protein for bio-active small molecule using photo-cross linked beads and MALDI-TOF mass spectrometry. Bio-protocol *10*, e3517.

Thomas, S., Sharma, N., Gonzalez, R., Pao, P.W., Hofman, F.M., Chen, T.C., Louie, S.G., Pirrung, M.C., and Schonthal, A.H. (2013). Repositioning of Verrucosidin, a purported inhibitor of chaperone protein GRP78, as an inhibitor of mitochondrial electron transport chain complex I. PLoS One *8*, e65695.

Tian, C., Clauser, K.R., Öhlund, D., Rickelt, S., Huang, Y., Gupta, M., Mani, D.R., Carr, S.A., Tuveson, D.A., and Hynes, R.O. (2019). Proteomic analyses of ECM during pancreatic ductal adenocarcinoma progression reveal different contributions by tumor and stromal cells. Proc. Natl. Acad. Sci. U S A *116*, 19609–19618.

von Ahrens, D., Bhagat, T.D., Nagrath, D., Maitra, A., and Verma, A. (2017). The role of stromal cancer-associated fibroblasts in pancreatic cancer. J. Hematol. Oncol. *10*, 76.

Wang, D.S., Jonker, J.W., Kato, Y., Kusuhara, H., Schinkel, A.H., and Sugiyama, Y. (2002). Involvement of organic cation transporter 1 in hepatic and intestinal distribution of metformin. J. Pharmacol. Exp. Ther. *302*, 510–515.

Webb, B.A., Chimenti, M., Jacobson, M.P., and Barber, D.L. (2011). Dysregulated pH: a perfect storm for cancer progression. Nat. Rev. Cancer *11*, 671–677.

Yamori, T. (2003). Panel of human cancer cell lines provides valuable database for drug discovery and bioinformatics. Cancer Chemother. Pharmacol. *52*, S74–S79.

Yoshida, J., Abe, H., Watanabe, T., and Kawada, M. (2018). Intervenolin suppresses gastric cancer cell growth through the induction of TSP-1 secretion from fibroblast-like stromal cells. Oncol. Lett. *16*, 6777–6785.

Zhang, D., Li, L., Jiang, H., Li, Q., Wang-Gillam, A., Yu, J., Head, R., Liu, J., Ruzinova, M.B., and Lim, K.H. (2018). Tumor-stroma IL1β-IRAK4 feedforward circuitry drives tumor fibrosis, chemoresistance, and poor prognosis in pancreatic cancer. Cancer Res. *78*, 1700–1712.

Zhang, S., Reljić, B., Liang, C., Kerouanton, B., Francisco, J.C., Peh, J.H., Mary, C., Jagannathan, N.S., Olexiouk, V., Tang, C., et al. (2020). Mitochondrial peptide BRAWNIN is essential for vertebrate respiratory complex III assembly. Nat. Commun. *11*, 1312.

Zhang, Y., Guo, H., Guo, X., Ge, D., Shi, Y., Lu, X., Lu, J., Chen, J., Ding, F., and Zhang, Q. (2019). Involvement of Akt/mTOR in the neurotoxicity of rotenone-induced Parkinson's disease models. Int. J. Environ. Res. Public Health *16*, 3811.

Zhou, X., Kuang, Y., Liang, S., and Wang, L. (2019). Metformin inhibits cell proliferation in SKM-1 cells via AMPK-mediated cell cycle arrest. J. Pharmacol. Sci. *141*, 146–152.

STAR★METHODS

KEY RESOURCES TABLE

REAGENT or RESOURCE	SOURCE	IDENTIFIER
Antibodies		
Anti-phospho-(T389)-p70S6 kinase	Cell signaling Technology	Cat#9234; RRID: AB_2269803
Anti-phospho-(S235/236)-S6 Ribosomal Protein	Cell signaling Technology	Cat#2211; RRID: AB_331679
Anti-phospho-(T172)-AMPK alpha	Cell signaling Technology	Cat#2535; RRID: AB_331250
Anti-AMPK alpha1	Cell signaling Technology	Cat#2795; RRID: AB_560856
Anti-PP2A C subunit	Cell signaling Technology	Cat#2259; RRID: AB_561239
Anti-GAPDH	Cell signaling Technology	Cat#5174; RRID: AB_10622025
Anti-phospho-(S473)-Akt	Cell signaling Technology	Cat#4060; RRID: AB_2315049
Anti-p70S6 kinase	Santa Cruz Biotechnology	Cat#SC-230; RRID: AB_632156
Anti-phospho-(T202/Y204)-ERK1/2	Santa Cruz Biotechnology	Cat#SC-7383; RRID: AB_627545
Anti-NDUFB8	Abcam	Cat#ab110242; RRID: AB_10859122
Anti-α-tubulin	Sigma-Aldrich	Cat#T5168; RRID: AB_477579
Anti-rabbit IgG peroxidase-linked whole antibodies from donkey	GE Healthcare	Cat#NA 934; RRID: AB_772206
Anti-mouse IgG peroxidase-linked whole antibodies from donkey	GE Healthcare	Cat#NA 931; RRID: AB_772210
Anti-LAMP1	Abcam	Cat#ab25630; RRID: AB_470708
anti-mTOR	Cell Signaling Technology	Cat#2983; RRID: AB_2105622
Alexa Fluor 546 anti-Mouse IgG	Thermo Fisher Scientific	Cat#A-21123; RRID: AB_2535765
Alexa Fluor 488 anti-Rabbit IgG	Thermo Fisher Scientific	Cat#A-21206; RRID: AB_2535792
Anti-a-SMA	Abcam	Cat#ab7817; RRID: AB_262054
Anti-Vimentin	Santa Cruz Biotechnology	Cat#sc-6260; RRID: AB_628437
Anti-GFP	Cell Signaling Technology	Cat#2955; RRID: AB_1196614
Anti-Ki-67	Abcam	Cat#ab16667; RRID: AB_302459
Anti-Phospho-p70 S6 Kinase (Thr 389)	Aviva Systems Biology	Cat#OAAF07416; RRID: AB_2630782
Anti-HLA	Hokudo	Cat#AB-46; RRID: AB_1962147
Anti-BrdU	Dako	Cat#M0744; RRID: AB_10013660
Anti-S6K	Santa Cruz Biotechnology	Cat#sc-8418; RRID: AB_628094
Biological samples		
Mouse tumor tissue	This manuscript	N/A
Tissue samples from PDAC patients and PDX mouse	JFCR	approval number 2012-1001
Chemicals, peptides, and recombinant proteins		
Metformin	Sigma-Aldrich	D150959
Rotenone	Sigma-Aldrich	R8875
Arctigenin	Sigma-Aldrich	SMB00075
Buformin hydrocjloride	Santa Cruz Biotechnology	sc-207383
NADH	Sigma-Aldrich	N8129
Ubiquinone	Sigma-Aldrich	C7956
Sodium L-lactate	Sigma-Aldrich	71718
L-(+)-Lactic acid	Sigma-Aldrich	L1750
Calyculin A	Cell Signaling Technology	9902

(*Continued on next page*)

Continued

REAGENT or RESOURCE	SOURCE	IDENTIFIER
Temsirolimus	Sigma-Aldrich	PZ0020
Nigericin	Sigma-Aldrich	N7143
TTFA (2-thenoyltrifluoroacetone	Sigma-Aldrich	T27006
KCN (potassium cyanide	Sigma-Aldrich	60178
Antimycin A	Sigma-Aldrich	A8674
Oligomycin	Sigma-Aldrich	O4876
ASP4132	Synthesized	(Kuramoto et al., 2020)
MTT	DOJINDO	341-01823
Matrigel	BD Biosciences	354230
ITV- and AS-1936-immobilized beads	This manuscript	N/A
Guide-it Recombinant Cas9 protein	Z2641N	TaKaRa Bio
pHrodo Red AM	Thermo Fisher Scientific	P35372
Masson's Trichrome staining	Sigma-Aldrich	HT15
Critical commercial assays		
XF mitostress kit	Agilent Technologies	103-015-100
MitoXpress	Agilent Technologies	MX-200-4
Mitochondria Isolation Kit	Abcam	ab110171
MitoCheck Complex Activity Assay Kit	Cayman Chemical	#700939, #700940, #700950, #700990, #701000
Lactate Assay Kit II	BioVision	K627-100
Lactate-Glo Assay	Promega	J5021
LabAssay Glucose	Wako	298065701
Proteome Profiler Human Phospho-Kinase Array Kit	R&D systems	ARY003C
ChemMate EnVision kit	Dako	K5007
Envision + Dual Link System-HRP	Dako	K4063
Liquid DAB + Substrate Chromogen System	Dako	K3468
BrdU solution	BD Biosciences	550891
PI/RNase Staining Buffer	BD Biosciences	550825
Experimental models: Cell lines		
MKN-1	JCRB	JCRB0252
MKN-B	JCRB	JCRB1025
MKN-74	JCRB	JCRB0255
DLD-1	ATCC	CCL-221
HCT-15	ATCC	CCL-225
HCT-116	ATCC	CCL-247
A549	ATCC	CCL-185
NCI-H23	ATCC	CRL-5800
DMS 273	ECACC	95062830
LNCaP	ATCC	CRL-1740
DU-145	ATCC	HTB-81
PC-3	ATCC	CRL-1435
Capan-1	ATCC	HTB-79
MIA PaCa-2	ATCC	CRL-1420
BxPC-3	ATCC	CRL-1687
CCD-18Co	ATCC	CRL-1459

(*Continued on next page*)

Continued

REAGENT or RESOURCE	SOURCE	IDENTIFIER
NHLF	Lonza	CC-2512
PrSC	Lonza	CC-2508
HPaSteC	ScienCell Research Laboratories	#5301
Hs738	ATCC	CRL-7869
Experimental models: Organisms/strains		
Mouse: CAnN.Cg-*Foxn1*^{nu}/CrlCrlj (BALB/c nude)	Charles River Laboratories	https://www.crj.co.jp/product/rm/detail/balbcnu
Mouse: NOD.CB17-*Prkdc*^{scid}/J (NOD-SCID)	Charles River Laboratories	https://www.crj.co.jp/product/rm/detail/nodscid
Mouse: Nod.Cg-*Prkdc*^{scid}*IL2rg*^{tm1Wjl}/SzJ (NSG)	Charles River Laboratories	https://www.crj.co.jp/product/rm/detail/nsg
PDX model	JFCR	approval number 2012-1001
Oligonucleotides		
ON-TARGETplus siRNA-SMARTpool, Non-targeting Pool	Dharmacon	D-001810-10-15
ON-TARGETplus siRNA-SMARTpool, PPP2CA	Dharmacon	L-003598-01-0005
ON-TARGETplus siRNA-SMARTpool, PPP2CB	Dharmacon	L-003599-00-0005
crRNA, GPR132		UAAGUGGCCCGUUGAUUCGU and UGCUGGUGAGGGGUCCGUAC
tracrRNA	Sigma-Aldrich	TRACRRNA05N-5NMOL
GPR4 primers for qPCR	TaKaRa Bio	HA104269
GPR65 primers for qPCR	TaKaRa Bio	HA159373
GPR68 primers for qPCR	TaKaRa Bio	HA274097
GPR132 primers for qPCR	TaKaRa Bio	HA274259
GAPDH primers for qPCR	TaKaRa Bio	HA067812
Software and algorithms		
ImageJ	NIH	https://imagej.nih.gov/ij/
FACSuite software (version 1.2.1)	BD Biosciences	https://www.bdbiosciences.com/ja-jp/products/software/instrument-software/bd-facsuite-application#Overview

RESOURCE AVAILABILITY

Lead contact

Further information and requests for resources and reagents should be directed to and will be fulfilled by the lead contact, Manabu Kawada (kawadam@bikaken.or.jp)

Materials availability

ITV-and AS-1936-immobilized beads are available by the lead contact upon request.

Data and code availability

All data reported in this paper will be shared by the lead contact upon request.

This paper does not report original code.

Any additional information required to reanalyze the data reported in this paper is available from the lead contact upon request.

EXPERIMENTAL MODEL AND SUBJECT DETAILS

Animals

Mouse xenograft model. All animal studies were approved by the Institutional Committee for Animal Experiments of the Institute of Microbial Chemistry and performed in accordance with the relevant

guidelines and regulations to minimize animal suffering. The anti-tumor activity of ITV was evaluated *in vivo* as previously mentioned (Kawada et al., 2013). Female BALB/c nude mice (5-week-old, $n = 5$) were purchased from Charles River Laboratories (Kanagawa, Japan) and used at 8 weeks of age.

Mouse PDX model. Male NOD.CB17-*Prkdc*^{scid}/J (NOD-SCID) mice and female Nod.Cg-*Prkdc*^{scid}*IL2rg*^{tm1Wjl}/SzJ (NSG) mice were purchased from Charles River Laboratories Japan (Kanagawa, Japan). All animal procedures were performed according to protocols approved by the Japanese Foundation for Cancer Research Animal Care and Use Committee (JFCR; approval number 18-01-3) and were in accordance with the relevant guidelines and regulations. Mice were housed in specific pathogen-free conditions. Tissue samples were obtained from PDAC patients in accordance with the guidelines of the JFCR (approval number 2012-1001). Informed consent was obtained from all patients.

Tissue for the PDX was derived from a CA19-9 and MUC-1 positive moderately differentiated PDAC tumor (KRAS mutated; Gly12Arg) obtained from a patient (female, aged 43) who underwent surgical resection at the Cancer Institute Hospital of JFCR. Tumor samples were processed within 24 h of biopsy. Then, tumor tissues were subcutaneously implanted into a 5–6-week-old NOD-SCID male mouse, and PDX were expanded in 5–6-week-old NSG female mice; excess tissues were frozen in CELLBANKER.

Cell culture. Human gastric cancer cell lines MKN-1, MKN-B, and MKN-74; human colorectal cancer cell lines DLD-1, HCT-15, and HCT-116; human lung cancer cell lines A549, NCI-H23, and DMS 273; human prostate cancer cell lines LNCaP-CR, DU-145, and PC-3; human pancreatic cancer cell lines Capan-1, MIA PaCa-2, and BxPC-3; and stromal cells CCD-18Co, NHLF, PrSC, and HPaSteC were obtained as previously described (Kawada et al., 2015; Nishiya et al., 2021). These cancer cell lines stably express a transfected GFP vector as previously described (12). Cancer cell lines were maintained in Dulbecco's modified Eagle's medium (DMEM; 05919, Nissui, Tokyo, Japan) supplemented with 10% fetal bovine serum (FBS, Sigma-Aldrich, St. Louis, MO), 100 U/mL penicillin G, 100 μg/mL streptomycin, and 0.292 mg/mL glutamine (10378-016, Thermo Fisher Scientific, Walthum, MA) at 37°C with 5% CO_2. Hs738.St/Int (Hs738) human gastric stromal cells (CRL-7869) were obtained from the American Type Culture Collection. Stromal cells were maintained in DMEM supplemented with 10% FBS, 100 U/mL penicillin G, 100 μg/mL streptomycin, 0.292 mg/mL glutamine, insulin/transferrin/hydrocortisone (ITH: 5 μg/mL insulin, 5 μg/mL transferrin, and 1.4 μM hydrocortisone), and 5 ng/mL basic FGF (PeproTech, Rocky Hill, NJ) at 37°C with 5% CO_2 (12). The preparation of the CM from stromal cells and the synthesis of ITV and its derivatives have been previously described (Abe et al., 2013a, 2013b).

METHOD DETAILS

Reagents

The reagents used and synthesized in this study were as follows: metformin (1,1-dimethylbiguanide hydrochloride: D150959, Sigma-Aldrich), rotenone (R8875, Sigma-Aldrich), arctigenin (SMB00075, Sigma-Aldrich), buformin (buformin hydrocjloride: sc-207383, Santa Cruz Biotechnology, Dallas, TX), NADH (N8129, Sigma-Aldrich), ubiquinone (coenzymeQ_1: C7956, Sigma-Aldrich), sodium lactate (sodium L-lactate, 71718, Sigma-Aldrich), lactate (L-(+)-Lactic acid, L1750, Sigma-Aldrich), calyculin A (#9902, Cell Signaling Technology, Danvers, MA), temsirolimus (PZ0020, Sigma-Aldrich), nigericin (N7143, Sigma-Aldrich), TTFA (2-thenoyltrifluoroacetone, T27006, Sigma-Aldrich), KCN (potassium cyanide, 60178, Sigma-Aldrich), antimycin A (A8674, Sigma-Aldrich), and oligomycin (O4876, Sigma-Aldrich). ASP4132 was synthesized as previously described (Kuramoto et al., 2020).

Cell viability assays

Cells were inoculated into 96-well plates at 5×10^3 cells per well in 0.1 mL of DMEM supplemented with 1% dialyzed FBS (D-FBS) and ITH. After culture for the indicated number of days, cell growth was determined using 3-(4,5-dimethyl-2-lythiazolyl)-2,5-diphenyl-2*H*-tetrazolium bromide (MTT; 341-01823, DOJINDO, Kumamoto, Japan) assay (12). Alternatively, cells were lysed in 10 mm Tris–HCl at pH 7.4 containing 150 mm NaCl, 0.9 mm $CaCl_2$, and 1% Triton X-100, and cell growth was measured based on GFP fluorescence intensity (excitation wavelength at 485 nm and emission wavelength at 538 nm) and assessed using a Cytation 5 plate reader (BioTek, Winooski, VT). Co-culture experiments and the evaluation of mode of action of the compounds using the JFCR 39 cell-line panel were performed as previously described (Kawada et al., 2015; Nakatsu et al., 2007).

Mouse xenograft models

Cancer cells (8×10^6) were suspended with or without the indicated stromal cells (8×10^6) in 0.3 mL of 10% FBS-DMEM and mixed with 0.5 mL of BD Matrigel Matrix Growth Factor Reduced (BD Biosciences Systems, Franklin Lakes, NJ), 100 μL of which (1×10^6) was subcutaneously injected into the left lateral flank of BALB/c nude mice. The vehicle (saline supplemented with 10% DMSO and 1% Tween 80) or the indicated samples were intravenously (for ITV) or intraperitoneally (for ASP4132) administered 5 days a week to mice. Tumor volume was estimated using the following formula: tumor volume (mm) = (length × width^2)/2. Mice were euthanized on day 17 or 21 after cell implantation by cervical dislocation, and tumor weights were determined.

To evaluate the mechanism of action (Figure 6), three mice were used for each experimental set. After 24 h fasting, the vehicle or the indicated samples were intravenously administered into mice at 14 and 15 days after MKN-74 cell implantation. After 4 h, the mice were anesthetized with an intraperitoneal injection of mixed anesthesia containing medetomidine hydrochloride (0.75 mg/kg, Kyoritsu Seiyaku, Tokyo, Japan), midazolam (4 mg/kg, Sandoz, Tokyo, Japan), and butorphanol tartrate (5 mg/kg, Meiji Seika Pharma, Tokyo, Japan).

Isolation of mouse fibroblasts

Tumors were excised from euthanized mice, cut into small pieces (approximately 1 mm^3), and cultured on a 35 mm dish with a drop of FBS. After air-drying, the tumor pieces were cultured in DMEM containing 1% D-FBS and ITH. After fibroblast expansion, they were trypsinized and pooled for further use.

OCR and extracellular acidification

Metabolic analysis was performed using Seahorse XFe24 analyzer (Agilent Technologies, Santa Clara, CA). Gastric cancer cells were cultured in 24-well plates for XFe24, and MKN-B cells (5×10^5) and the growth medium (2×10^5 cells/250 μL) were added. After equilibration in non-CO_2 incubator for 1 h, the medium was replaced with 450 μL of the assay medium (XF DMEM, 103575-100, Agilent Technologies; containing 10 mm glucose, 1 mm pyruvate, and 2 mm glutamine). Mitostress test was performed with ITV (final concentration: 0.25, 0.5, and 1 μg/mL), FCCP (1 μM), and rotenone/antimycin A (0.5 μM).

For glucose-depleted conditions, the assay medium without glucose and pyruvate was used. Analysis was performed 1 h after incubation and after treatment with ITV (1 μg/mL), rotenone (0.01 μg/mL), glucose (16.7 mM), and succinate (30 mM). FCCP, rotenone, and antimycin A were purchased from Agilent Technologies (XF mitostress kit, 103015-100). MitoXpress (MX-200-4, Agilent) assay was performed according to manufacturers instructions. Cells (8×10^4 cells/well) were seeded in 96-well plates with the growth medium that was replaced with fresh medium containing 1% D-FBS with the MitoXpress reagent. The fluorescence signal of MitoXpress reagent was immediately read using a Cytation 5 plate reader after the addition of test compounds.

Enzymatic activity of complex I

Mitochondria were isolated from culture cells using a Mitochondria Isolation Kit (ab110171, Abcam, Cambridge, UK) according to manufacturer's instruction. Mitochondria extracts were frozen and thawed for three cycles. Protein concentration was determined using a protein assay (5000006JA, Bio-Rad Laboratories, Hercules, CA). For complex I activity assay, test compounds (20 μL) were added to 96-well plates, and mitochondria extract (5 μg) in 165 μL of assay buffer (containing 3.6 mg/mL fatty acid free BSA, 2.4 mg/mL antimycin A, 0.12 mM NADH, and 0.36 mM KCN in 60 mM potassium phosphate buffer at pH 7.5) was added to each well. After pre-heating the plate to 37°C and the addition of 15 μL of ubiquinone (1 mM), OD_{340} was immediately measured using Cytation 5 plate reader. The amount of reduced NADH was obtained by subtracting the value at 10 min from that at 5 min. The method for complex I activity assay was modified from a previous report (Spinazzi et al., 2012). To determine the activity of mitochondrial complexes I–V (Figure S3F), MitoCheck Complex Activity Assay Kit (#700939, #700940, #700950, #700990, #701000, Cayman Chemical, Ann Arbor, MI) was used according to manufacturer's instruction.

Pull-down assay

ITV- and AS-1936-immobilized beads were prepared (Kanoh et al., 2005; Suvarna et al., 2020). Mitochondrial fractions from Hs738 cells were resuspended in the lysis buffer used for western blotting and

incubated with ITV-conjugated beads for 3 h at 4°C. After washing the beads with 50 mM HEPES-KOH (at pH 7.5 containing 150 mM NaCl, 1 mM EDTA, and 2.5 mM EGTA), the beads were denatured in SDS sample buffer by boiling and subjected to western blot analysis.

Measurement of lactate and glucose levels

Lactate Assay Kit II (K627-100, BioVision, Milpitas, CA) was used to determine lactate levels in co-cultured CM and monocultured cells according to the manufacturer's instruction. Co-cultured CM was collected from the 96-well plates of co-culture experiment 3 days after the inoculation of cancer cells, whereas monocultured cells were seeded in 96-well plates (5×10^3 cells/well) in DMEM containing 1% D-FBS and ITH for 3 days. The supernatant of centrifuged CM (1,000 × *g*, 10 min at 25°C) and tissue samples from western blot analysis were used to measure lactate levels using Lactate-Glo Assay (J5021, Promega, Madison, WI). Extracellular glucose concentration of the CM from monocultured cells was measured using LabAssay Glucose (298065701, Wako, Tokyo, Japan).

Metabolite extraction and metabolomic analysis

Cells were seeded in 10 cm dishes (3×10^6 cells/dish) in DMEM with 10% FBS, and the medium was replaced with DMEM containing 1% D-FBS. Cells were incubated with the test compounds for 3 h while the control groups were treated with DMSO at equal concentrations. Then, cells were washed with mannitol solution and treated with 800 μL methanol for 30 s. The cell extract was added with 550 μL Milli-Q water containing internal standards (H3304-1002, Human Metabolome Technologies [HMT], Tsuruoka, Yamagata, Japan) for another 30 s. The obtained extract was centrifuged at 2,300 × *g* and 4°C for 5 min, after which 800 μL of the supernatant was centrifugally filtered at 9,100 × *g* and 4°C through a Millipore 5 kDa cutoff filter (Ultrafree MC-PLHCC, HMT). Metabolomic analysis was conducted with the *C-SCOPE* package of HMT using capillary electrophoresis time-of-flight mass spectrometry (CE-TOFMS) for cation analysis and CE-tandem mass spectrometry (CE-MS/MS) for anion analysis as previously described (Junker et al., 2006; Ohashi et al., 2008; Ooga et al., 2011; Sugimoto et al., 2010).

Western blot analysis

Cell lysates were prepared from cultured cells and subjected to western blotting with the following primary antibodies: anti-phospho-(T389)-p70S6 kinase (#9234), anti-phospho-(S235/236)-S6 Ribosomal Protein (#2211), anti-phospho-(T172)-AMPK alpha (#2535), anti-AMPK alpha1 (#2795), anti-PP2A C subunit (#2259), anti-GAPDH (#5174), and anti-phospho-(S473)-Akt (#4060), all from Cell Signaling Technology, anti-p70S6 kinase (SC-230, Santa Cruz Biotechnology), anti-phospho-(T202/Y204)-ERK1/2 (SC-7383, Santa Cruz Biotechnology), and NDUFB8 (ab110242, Abcam) (20). The following secondary antibodies were used: mouse monoclonal anti-α-tubulin (1:1,000 dilution; T5168; Sigma-Aldrich), anti-rabbit IgG peroxidase-linked whole antibodies from donkey (NA 934, GE Healthcare, Chicago, IL), and anti-mouse IgG peroxidase-linked whole antibodies from donkey (NA 931, GE Healthcare). Next, anti-phospho kinase antibody array was performed using a Proteome Profiler Human Phospho-Kinase Array Kit (ARY003C, R&D systems, Minneapolis, MN). MKN-74 cells were seeded in 6-well plates (3×10^4 cells/well) in DMEM supplemented with 1% D-FBS and cultured for 3 h, and the medium was replaced with the Ctrl CM or ITV CM.

siRNA transfection

For gene knockdown experiments, ON-TARGETplus siRNA-SMARTpool was used (Human PPP2CA: L-003598-01-0005, Human PPP2CB: L-003599-00-0005, Non-targeting Pool: D-001810-10-15, Dharmacon, Lafayette, CO). Lipofectamine RNAiMAX Reagent (13778, Thermo Fisher Scientific) was used for siRNA.

Immunofluorescence

Cells (1×10^5 cells/mL) were cultured on glass cover slips in 6-well plates in 2 mL of DMEM with 1% D-FBS, and the medium was replaced with the indicated prepared medium. Earle's balanced salt solution (EBSS) was purchased from Thermo Fisher Scientific (24010-043). Cells were washed with ice cold PBS (−) and fixed with 4% paraformaldehyde in PBS (−) for 10 min at 25°C. After washing with PBST (0.1% Tween-20 in PBS), cells were permeabilized with PBST-BSA (0.1% Tween-20, 0.1% BSA in PBS) for 45 min at 25°C and stained with DAPI, anti-LAMP1 (ab25630, Abcam), anti-mTOR (2983, Cell Signaling Technology) primary antibodies, and Alexa Fluor 546 anti-Mouse IgG (A-21123, Thermo Fisher Scientific) and Alexa Fluor 488 anti-Rabbit IgG (A-21206, Thermo Fisher Scientific) second antibodies. Stained cells were visualized under

an Axiovert 200M microscope using the LSM5 LIVE scanning module of the LSM LIVE DUO software (ZEISS, Oberkochen, Germany).

Gene knockout

MKN-74 cells were seeded in 6-well plates (1×10^5 cells/well) in 2 mL DMEM with 10% FBS. Two CRISPR RNAs (crRNAs) for each gene were designed by CRISPRdirect (70) and purchased from Sigma-Aldrich (crRNA sequence, GPR132: UAAGUGGCCCGUUGAUUCGU and UGCUGGUGAGGGGUCCGUAC). The ribonucleoprotein (RNP) was constructed using two crRNAs (60 pmol), 60 pmol SygRNA Synthetic tracrRNA (TRACRRNA05N-5NMOL, Sigma-Aldrich), and 3 μg Guide-it Recombinant Cas9 protein (Z2641N, TaKaRa Bio, Shiga, Japan). Next, RNP was mixed with 10 mm Tris buffer at pH 7.5 (T2319, Sigma-Aldrich) and incubated on ice for 30 min. For transfection, 5 μL TransIT-CRISPR (T1706, Sigma-Aldrich) in 250 μL OPTI-MEM (31985062, Thermo Fisher Scientific) was added to the RNP solution and cell culture medium after incubation for 20 min.

Quantitative PCR

RNA was isolated using an RNeasy kit (74004, QIAGEN, Hilden, Germany), and cDNA was synthesized using a Reverse Transcription System (A3500, Promega). Quantitative PCR was performed using GoTaq qPCR Master Mix (A6001, Promega) on a Thermal Cycler Dice Real Time System III (TaKaRa Bio). The primer sets were purchased from TaKaRa Bio (GPR4: HA104269, GPR65: HA159373, GPR68: HA274097, GPR132: HA274259, GAPDH: HA067812). Relative expression levels were calculated by the 2 (-Delta Delta C(T)) method (Livak and Schmittgen, 2001), and *GAPDH* was used as the reference gene.

Intracellular pH

Measurement of intracellular pH using pHrodo Red AM (P35372, Thermo Fisher Scientific) was performed. Cells were seeded into 96-well plates (3×10^4 cells/well) in 0.1 mL DMEM supplemented with 1% D-FBS, and the medium was replaced with 0.1 mL HBSS/HEPES buffer (1.2 mM $CaCl_2$, 0.8 mM $MgSO_4$, 5.4 mm KCl, 0.4 mM KH_2PO_4, 4.2 mM $NaHCO_3$, 137 mM NaCl, 0.3 mM Na_2HPO_4, 5.5 mM glucose, and 52 mM HEPES at pH 7.4) containing pHrodo Red and the test compound. After 3 h incubation in CO_2 incubator, the buffer was replaced with fresh buffer, and fluorescence intensity was determined using Cytation 5 plate reader.

Sample preparation from mouse tumor tissues

Tumor tissues were washed with ice cold PBS (without calcium and magnesium), and their weight was measured. Tumor tissues were homogenized in a Dounce homogenizer with RIPA buffer (150 mM NaCl, 1% Triton X-100, 0.5% sodium deoxycholate, 0.1% SDS, 1 mM EDTA, 10 mM NaF, and 50 mM Tris-HCl at pH 7.4), PhosSTOP (4906845001, Sigma-Aldrich), and 25 μg/mL each of antipain, leupeptin, and pepstatin. The collected supernatants from a half volume of lysate that were centrifuged at 15,000 rpm for 15 min at 4°C were subjected to western blot analysis. Next, 0.125 mL 0.6 N HCl was added to the other half volume of lysate and mixed by vortex. After the addition of 0.125 mL Trizma base (0.121 g/mL; Sigma-Aldrich) and vortexing at 15,000 rpm for 15 min at 4°C, samples were centrifuged, and then the supernatants were used for the lactate assay.

Histology and immunohistochemistry

Immunohistochemical analysis for mouse xenograft model was performed as previously described (Ohishi et al., 2018). Briefly, paraffin-embedded tissues were cut and mounted on slides. To deplete paraffin, the sections were washed with xylene, ethanol, and methanol hydrogen peroxide. The deparaffinized sections were boiled in 0.01 M buffered sodium citrate solution (pH 6.0) for 10 min and subjected to Masson's Trichrome staining (Sigma-Aldrich) overnight or immunohistochemical staining with the following antibodies for 30 min: anti-a-SMA (1:2000, ab7817, Abcam), anti-Vimentin (1:400, sc-6260, Santa Cruz Biotechnology), anti-GFP (1:500, #2955, Cell Signaling Technology), anti-Ki-67 (1:200, ab16667, Abcam), anti-Phospho-p70 S6 Kinase (Thr 389) (1:50, OAAF07416, Aviva Systems Biology, San Diego, CA), and horseradish peroxidase-linked secondary antibodies. Tissues were stained with 3,3′-diaminobenzidine (DAB) using a ChemMate EnVision kit (Dako, Carpinteria, CA), counterstained with hematoxylin, visualized under a Nikon Biophot microscope (Tokyo, Japan), and photographed using a digital camera (Nikon Digital Sight DS- Ri1).

For the PDX model, tumors were fixed with 4% paraformaldehyde solution, embedded in paraffin, cut into 2 to 4 μm-thick sections, de-paraffinized with xylene, re-hydrated using graded ethanol, and subjected to

hematoxylin and eosin (HE) staining or the subsequent immunohistochemistry. Antigen retrieval was performed using microwave heating for 10 min in sodium citrate-hydrochloric acid buffer (10 mM, pH 6.0). After rinsing in PBS, the sections were incubated with the primary antibodies overnight at 4°C. Thereafter, immunohistochemical staining was performed using a DAKO Envision + Dual Link System-HRP (K4063, Dako) with Liquid DAB + Substrate Chromogen System (K3468, Dako) and counterstained with hematoxylin. The following antibodies were used: anti-HLA (AB-46, Hokudo, Hokkaido, Japan), anti-BrdU (M0744, Dako), anti-S6K (sc-8418, Santa Cruz Biotechnology), and anti-phospho-S6RP(Ser235/236) (#2211, Cell Signaling Technology).

BrdU labeling assay

5-Bromo-2′-deoxyuridine (BrdU) labeling assay was conducted to evaluate tumor cell proliferation. At the end of experiments, animals were intraperitoneally injected with 0.2 mL of 10 mg/mL BrdU solution (550891, BD Biosciences) 90 min before euthanization. Paraffin-embedded tissue sections were immunostained using monoclonal antibodies against BrdU (M0744, Dako) and imaged using an ECLIPSE TE2000-U microscope (Nikon).

PDX model

When the tumor volume reached 200 mm^3, mice were randomly divided into two groups administered with ITV (12.5 mg/kg in 100 μL saline containing 10% DMSO and 1% Tween 80) or the vehicle via the tail vain every 5 days except during weekends for a total of 2.5 weeks. Tumor size was assessed twice weekly using a caliper [(length × $width^2$)/2]. Immunodeficient mice were then euthanized 18 days after ITV treatment. The areas containing the transplanted tumor tissues of PDX were measured and weighed.

Flow cytometry

Cultured cells were collected by trypsinization and fixed with cold 70% ethanol. After 2 h incubation in ice, cells were washed with PBS and stained with propidium iodide (PI/RNase Staining Buffer, 550825, BD Biosciences) for 15 min according to manufacturer's instruction. PI intensity was analyzed using BD FACSLyric flow cytometer (BD Biosciences). Data analysis was performed using the BD FACSuite software (version 1.2.1, BD Biosciences).

QUANTIFICATION AND STATISTICAL ANALYSIS

Statistical analysis was performed using two-tailed Student's *t*-test. Data are representative of at least three independent experiments. All data are presented as the mean ± standard deviation (s.d.). The number of replicates (*n*) and p values are indicated in each figure legend. A p value of <0.05 was considered to be statistically significant.